KUNGLIGA TEKNISKA HÖGSKOLAN
& POLITECNICO DI TORINO

MSc program in Vehicle Engineering (KTH)
MSc program in Automotive Engineering (PoliTO)
A.Y. 2024/25

November 21, 2025

Torque Vectoring control system for a Formula Student vehicle

Supervisors:
Prof. Mikael Nybacka (KTH)
Prof. Aldo Sorniotti (PoliTO)

Author:
Carlo Vittorio Colucci

Abstract

Mechatronic systems are powerful tools that allow to improve the vehicle stability and handling, by the implementation of automatic control strategies. The Torque Vectoring (TV) control belongs to this category: it exploits the allocation of the torque per each wheel, to control the global vehicle rotation.
Two different strategies are investigated for the control of the global vehicle rotation: one very simple to implement and to tune but primitive, based only on the steering wheel input, and another one more oriented on the vehicle handling optimization, still keeping an easy integration, known as Direct Yaw moment Control (DYC).
Also for the torque allocation, two algorithms with the same targets, but of different types, are discussed: one is rule-based, light from the computational point of view, but less accurate when it comes to constraints to respect and criteria to satisfy; the other one is based on an optimization problem, introducing an easy interface with the external constraints and input, but a more complex set-up and a heavier computational demand.
The logic and the theory behind each strategy, along with their implementation, are introduced. The control system simulation results are presented, and eventually discussed, by the aid of relevant performance parameters.

Sammanfattning

Mekatroniska system är kraftfulla verktyg som möjliggör förbättrad fordonsstabilitet och hantering genom implementering av automatiska styrstrategier. Torque Vectoring (TV)-kontroll tillhör denna kategori: den utnyttjar fördelningen av vridmomentet på varje hjul för att kontrollera fordonets globala rotation.
Två olika strategier undersöks för kontrollen av fordonets globala rotation: en som är enkel att implementera och justera men ganska primitiv, baserad enbart på rattens styrinmatning, och en annan som är mer inriktad på optimering av fordonsdynamiken, samtidigt som den bibehåller en enkel integration, känd som Direct Yaw moment Control (DYC).
Även för vridmomentsfördelningen diskuteras två algoritmer med samma mål, men av olika typer: den ena är rule-based, relativt lätt ur beräkningssynpunkt men mindre exakt när det gäller att respektera begränsningar och uppfylla kriterier; den andra är baserad på ett optimeringsproblem, vilket ger ett enkelt gränssnitt mot externa begränsningar och indata, men innebär en mer komplex uppsättning samt högre beräkningsbelastning.
Logiken och teorin bakom varje strategi, tillsammans med deras implementation, introduceras. Resultaten från simulering av styrsystemet presenteras och diskuteras slutligen med hjälp av relevanta prestandaparametrar.

Acknowledgment

I want to express my gratitude to myself for my strength of mind. I persevered to achieve my goals and dreams, showing resilience in facing and overcoming difficulties. I remained morally consistent with myself and successfully completed a challenging yet extraordinary journey; all while genuinely enjoying every moment.

I was fortunate to have the right people by my side to give me the support I needed and to guide me along the way, as well as the more negative ones who taught me how to be ready for life and grow as a person. This achievement is yours as well.

I'm grateful to Assunta and Romano, my parents, who believed in me every single day, constantly making me feel their unconditional love and belief in me. Life and challenges are easier with the awareness of such strength holding you.

Thank you, dear friends of mine; we have loved and continue to love each other as brothers. We shared this journey together, and we built amazing memories that will fill my heart forever. You guys shaped me into a better person.

Thank you, Cecilia, for unconditionally believing in me from the very first moment. I'm glad to have such a charismatic mentor beside me. Your energy and contagious positivity have had a significant influence on my perspective.

Finally, I am thankful to my Professors who instilled in me their knowledge and curiosity to discover more, who believed in my potential and strengthened my self-confidence. You have not only made me an engineer but also a more dynamic and grounded person. A special thank you to Daniel Arnström. Despite not being my professor or in any way related to the project, he cared about its evolution, teaching me various valuable tricks that have been crucial for the eventual success of the activity.

Contents

1 Introduction

This Master's thesis project presents the development of a vehicle Control System oriented to improve handling, stability and performance capabilities.
The work has been undertaken within the KTH Formula Student team, more specifically in the Vehicle Dynamics subgroup.

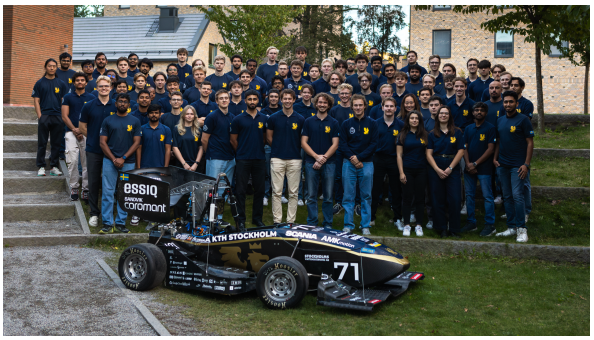

Figure 1: *KTH Formula Student team 2024/2025.*

Hereinafter, the Formula Student project is introduced and a presentation of the vehicle which has been used as a base to develop the Control System.
Furthermore, the adopted development process is explained, and the main sustainability topics and the limitations of the work are discussed.

1.1 What Formula Student is

Formula Student (FS) is a single-seat vehicle category, where teams, entirely made up of university students, compete to realize the fastest and most innovative prototype.
During the year each team works independently in synergy to design and to improve the new competing prototype to participate in the official competitions.
Each team presents a different internal organization, but a generic common structure, made up of different subgroups and a board, is identified. The KTH FS team is split into 6 different subgroups administered by a Team Captain:

- Aerodynamics and Composite (AC);
- Driverless (DV);
- Business & Management (BM);
- Mechanical Design (MD);
- Power Electronics (PE);
- Vehicle Dynamics (VD).

1.2 DeV19

The FS vehicle used as a test bench for this project is the Brinell DeV19.
The drivetrain is a fully electric four-wheel-drive system, with hub motors. The power is limited by the rulebook to $80kW$ (about $110hp$), with a power-to-weight ratio of about $320kW/t$ (against $185kW/t$ of a 2025 BMW M4).
The chassis is a full carbon-fiber monocoque.
The suspension system is a double wishbone with push-rod and decoupled heave and roll motion passive control.
Disk hub brakes are used for each wheel.
The vehicle also presents embedded systems for the autonomous drive mode.
The main parameters characterizing the vehicle are summarized in the following table:

Table 1: *DeV19 parameters.*

Parameter	Symbol	Value
Wheelbase	l	$1.535m$
Weight distribution (front)	w_d	46%
Center of gravity height	h_G	$0.28m$
Track width	t	$1.2m$
Tire radius	R	$0.23m$
Tire loaded radius	R_l	$0.22m$
Vehicle mass	M	$238kg$
Vertical polar moment of inertia	J_z	$115.4kg \cdot m^2$
Drag coefficient	C_x	1.56
Lift coefficient	C_z	3.65
Front section	S	$1.16m^2$
Transmission ratio	τ_{GB}	1/14

The control software is designed by Simulink and then imported into the dSpace framework. During the building phase, the MATLAB/Simulink code is converted into C-code and subsequently into machine code. This part will be treated in more detail in Section 7. Eventually, the software is uploaded on the dSpace MicroAutoBox II embedded in the vehicle.
The frequency of the control software is $200Hz$. However, the inertial measurement unit (IMU) presents a measurement frequency of $50Hz$, therefore limiting the Control System operation rate.

1.3 Development process

Before getting deep into the presentation of the Control System, an overview of the followed development process is presented.
The particular typology adopted in this project is the V-model:

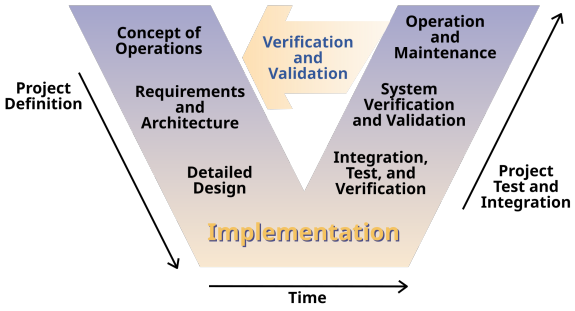

Figure 2: *V-model development process [1].*

Defining a proper work-flow is crucial to optimize productivity, according to the time available, and the quality of the resulting designed system.
Each Section is introduced following this particular process.
In particular, the concept of operations (Figure 2) is:

- Purpose and scope: what the system is intended to accomplish;
- Operational scenarios: how the system will be used;
- System boundaries: defining what is included and excluded in the system;
- Constraints and assumptions: any limitations or conditions that must be considered.

After this step, an analysis of the current state of the art is introduced: which are the most recent technologies developed by other researchers/car OEMs.

1.4 Sustainability

This project is related to two main sustainability topics: economic and environmental. The control system developed during this work is intended to improve the vehicle performance by optimizing the operation of the available sub-systems. Since it is deployed at software level, it does not require the manufacturing of any hardware components. No further sensors are required, apart from the common embedded ones on the vehicle. The accuracy and performance of the system could have been improved by implementing an optical vehicle speed sensor, but this would have significantly compromised the

economic sustainability.
Concerning the environmental sustainability, the control system can also be designed with the goal of optimizing the vehicle energy management. This feature can be implemented by controlling the torque on each wheel: the electric motor (EM) working point is shifted as close as possible to a high efficiency region.

1.5 Limitations of the project

As just explained in the previous Section, for economic reasons, the optical speed sensor has not been implemented. Therefore, the Control System is limited to operating with only one of the two relevant vehicle states of the lateral dynamics.

2 Concept of operations

The Torque Vectoring (TV) Control System is intended to improve handling, stability and performance by controlling the torque allocation for each wheel, depending on the driving conditions. The TV is an extension of the mechanical differential concept for all 4 wheels of the vehicle (Section 1.2).
It is enabled during all the testing sessions and during the Competition dynamic events, in particular for the Skidpad, Autocross and Endurance events.
The system deals with the control of the torque for each wheel, but does not take into account the current tire longitudinal slip. Therefore, it is interfaced with a Traction Control (TC), that provides the torque operational thresholds. Moreover, an Energy Efficient control imposes further constraints on the total torque demand.
The constraints/related rules stated by the FS rule-book are:

- the traction system power at the outlet of the Tractive System Accumulator Container (TSAC) must not exceed the value $P_{TSAC} = 80kW$;
- regenerating energy is allowed and unrestricted;
- wheels must not spin in reverse;
- a fully released accelerator pedal in manual mode must result in a wheel torque value $T \leq 0Nm$.

3 Requirements and architecture

To define some requirements the system must fulfill, data from an archive testing session are analyzed.
In particular, the fastest lap from a run of October 2024 is taken into account, with the following circuit layout (the scale on the axes is not to be taken as a reference):

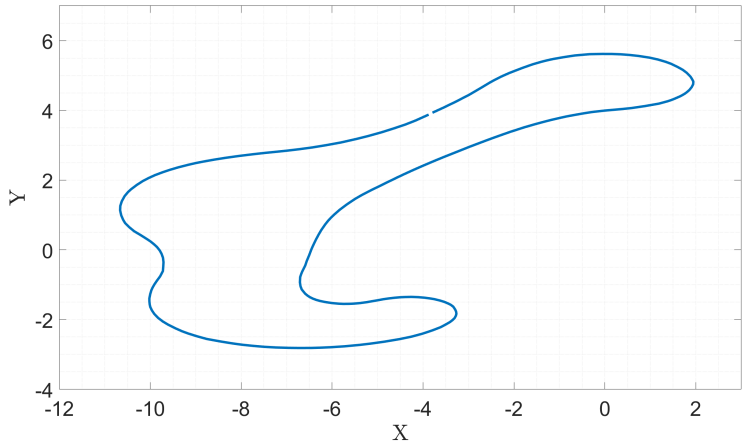

Figure 3: *Circuit layout.*

The trend of the main vehicle states during this lap is shown:

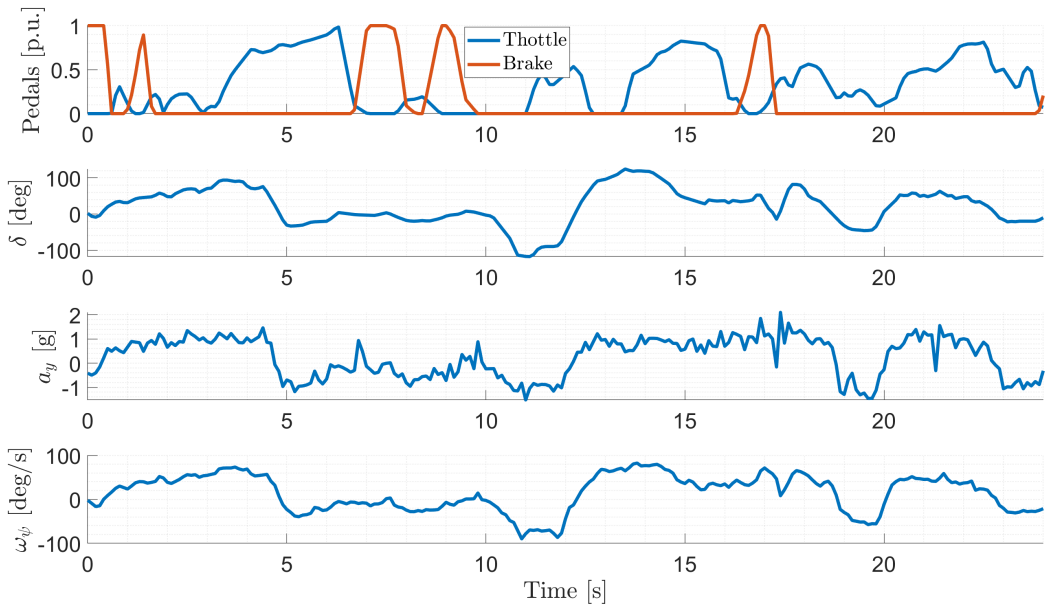

Figure 4: *Data lap, where pedals is the throttle and brake pedals position, δ is the steering wheel angle, a_y is the lateral acceleration and ω_ψ is the vehicle yaw rate.*

The maximum lateral acceleration experienced is $a_y^{MAX} = 2.1g$, while the average positive steering wheel angle is $\delta_{SW}^{AVG} = 51.6°$. Furthermore, starting from the yaw

rate data, the yaw acceleration and its maximum value are retrieved. Considering the vehicle yaw inertia $J_z = 115.4kg \cdot m^2$, the resulting maximum vehicle yaw moment is $N^{MAX} = 660Nm$.

3.1 Requirements

Beginning from the real values just retrieved by the testing session, precise targets are defined:

- increase of the maximum lateral acceleration by 10%: $a_{y,\,TV}^{MAX} \geq 2.3g$;
- reduction of the average steering wheel angle by 10%: $\delta_{SW,\,TV}^{AVG} \leq 46.4°$;
- reach a more neutral steering behavior.

Furthermore, the Control System is intended to easily handle the inputs and constraints coming from previous cascade controls: Power Limit Control, Traction Control, e-ABS, Energy Efficient Control, and other similar systems.

3.2 Architecture

Now that clear targets have been precisely set, the design of the Control System can be undertaken.
The Torque Vectoring architecture is split into two main parts:

- **Upper level control (ULC):** a specific controller (i.e. PID, LQR, etc.) is used to assess the vehicle amount of rotation. The input provided to the controller can be a current vehicle state or vehicle control input;
- **Lower level control (LLC):** control algorithm allocating the torques provided by the EMs on each wheel, to deliver the target rotation.

A more clear schematic of how the Control System is structured follows:

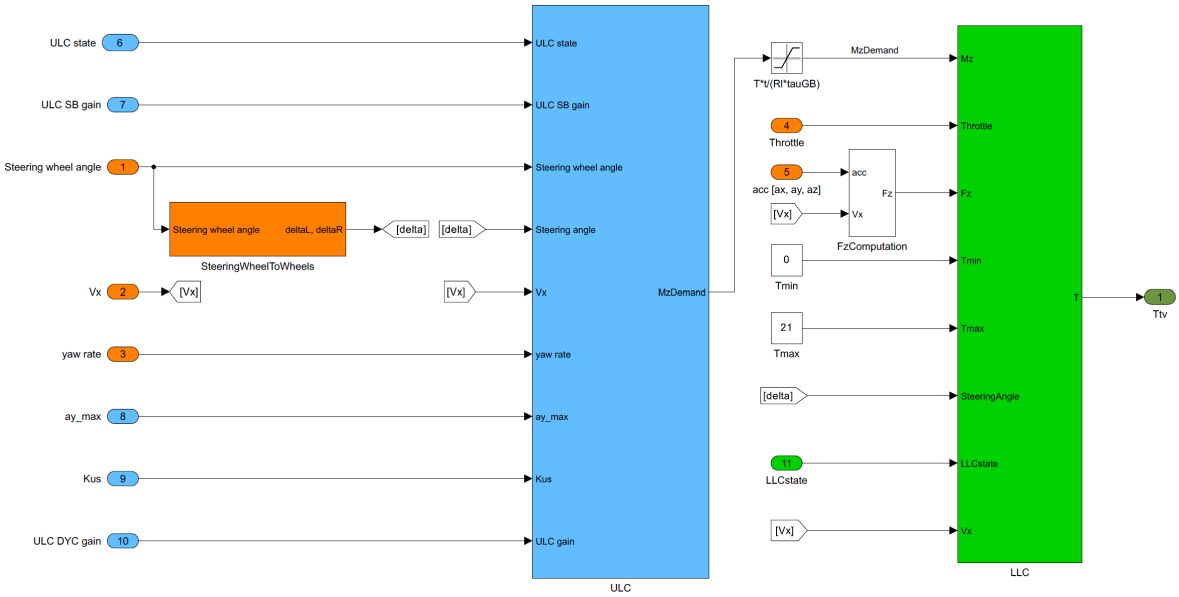

Figure 5: *TV architecture, where ULC is the blue subsystem and LLC is the green one.*

This architecture is used as a starting point to develop different logic of ULCs and LLCs, but before stepping into their design, a detailed explanation of the control flow follows:

1. Driver inputs

Throttle (h_a) and steering wheel angle (δ) are read from the CAN bus when the controller is integrated in a real scenario, or they are evaluated by means of a driver model within the simulation environment (Section 8.3). Once the driver inputs are read/generated, they are provided both to the ULC and to the LLC.
The throttle position determines the torque demand. The torque demand is the multiplication between the throttle percentage h_a and the maximum torque available, determined by the power limit ($80kW$) and the energy-efficient control:

$$T_{demand} = h_a \cdot T^{MAX}_{available} \tag{1}$$

2. From steering wheel angle to tire steering angles

Then, the steering wheel angle is used to evaluate the steering angles at tire level: the effective ones used by the LLC, and the vehicle model within the simulation environment. The conversion happens in two main steps:

- steering wheel angle to rack travel (l_r) by means of a gain (rack ratio $= 21$);
- rack travel to steering angles at tire level. Two separate look-up-tables (LUTs) are used to account for the difference between inner and outer wheel, due to the

Ackerman angle. The LUT values have been retrieved by means of the vehicle CAD model.

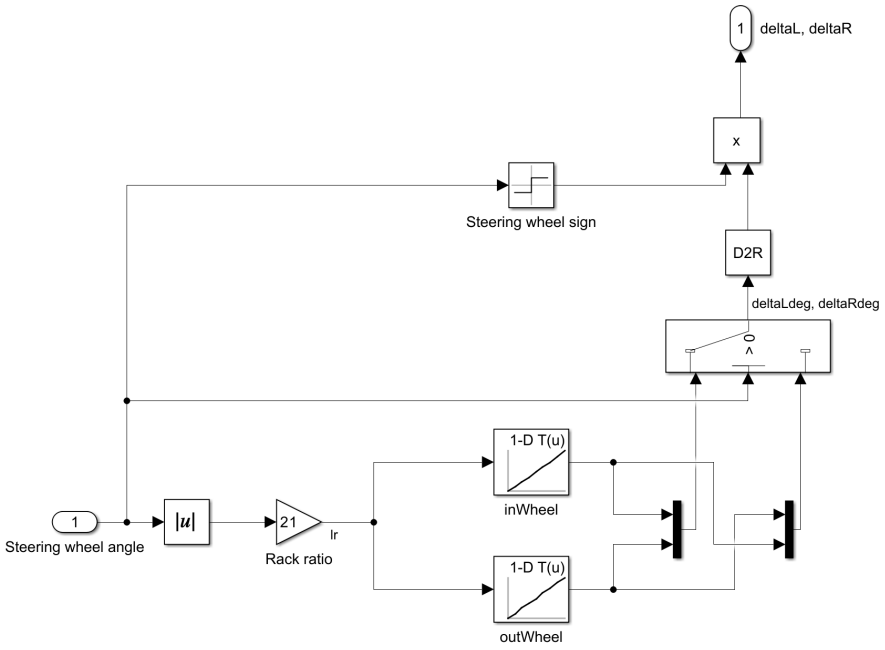

Figure 6: *Conversion system from steering wheel angle to tire steering angles.*

3. From accelerations to vertical loads

Another important step is the retrieval of the vertical loads that are provided to the LLC later on. The adopted approach is based on the following assumptions:

- the vehicle is considered to be fully rigid (i.e. with an infinitely rigid suspension system). This assumption is pretty strong and leads to overestimate the load transfer, since the presence of compliance would reduce it. Nevertheless, it still gives a reasonable and pretty accurate starting point, with a correct order of magnitude;
- the component of the force of gravity that appears in the equilibrium of moment when the vehicle rolls is neglected.

Starting with the description of the process, the accelerations in the three directions (a_x, a_y, a_z), measured by the Inertial Measurement Unit (IMU) or retrieved by vehicle simulation, result in the corresponding inertial forces:

$$F_x = M \cdot a_x; \quad F_y = M \cdot a_y; \quad F_z = M \cdot a_z \tag{2}$$

where M is the vehicle mass.
These forces are balanced by vertical forces on the four wheels. To compute them, an

equilibrium of forces and moments is undertaken according to the graphic representation shown below:

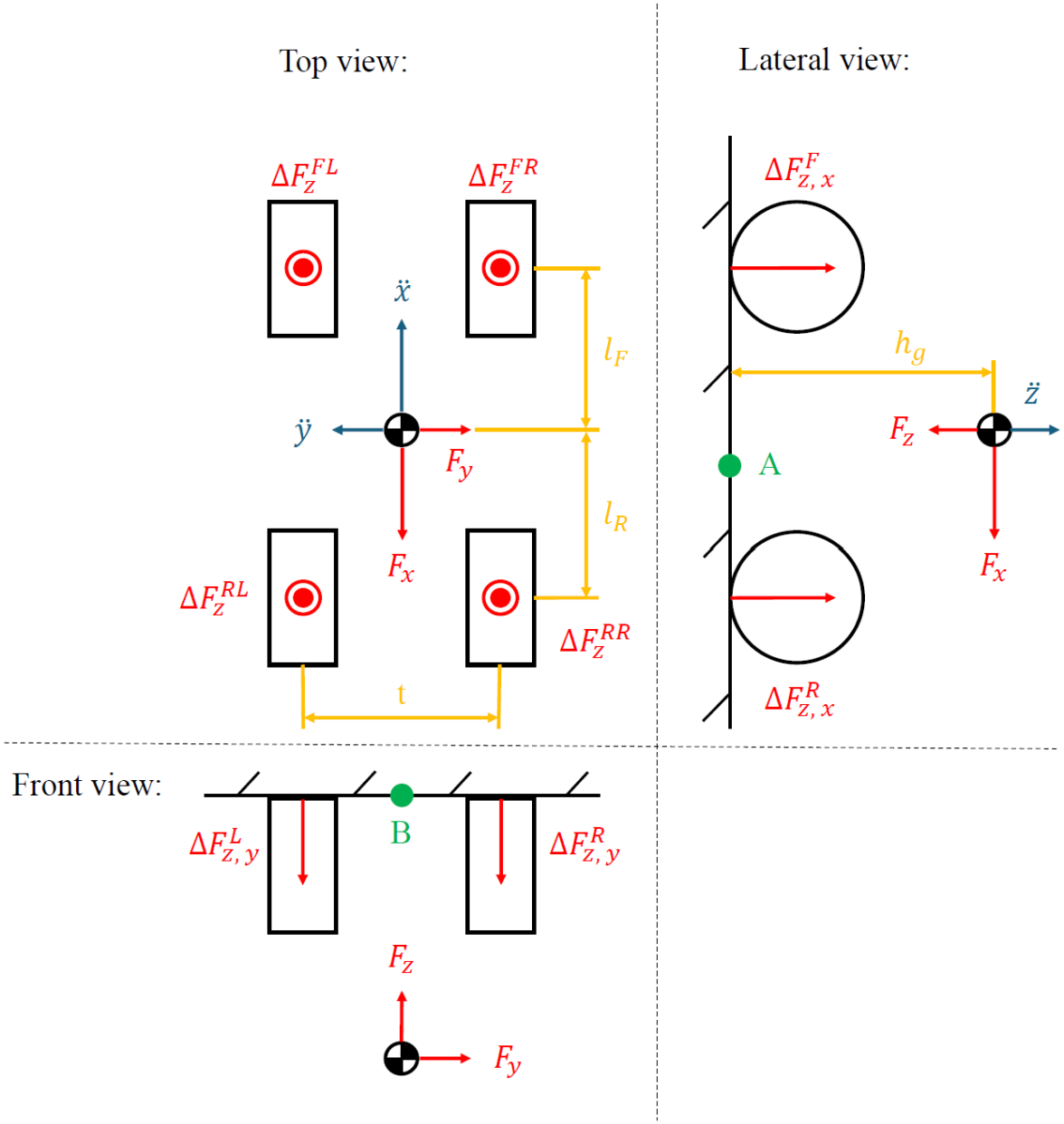

Figure 7: *Load transfer free body diagram.*

For the vertical inertial force, it is enough to equally split it on the four wheels:

$$\Delta F_{z,z}^{FL} = \Delta F_{z,z}^{FR} = \Delta F_{z,z}^{RL} = \Delta F_{z,z}^{RR} = \frac{F_z}{4} \tag{3}$$

The computed vertical forces are dynamic variations with respect to the static force of gravity, therefore they are denoted with the Δ symbol.
Considering the lateral view, the equilibrium around the point A results in the following vertical forces:

$$\Delta F_{z,x}^{F} = -F_x \cdot \frac{h_g}{l}; \quad \Delta F_{z,x}^{R} = -\Delta F_{z,x}^{F} \tag{4}$$

Instead, considering the front view, the equilibrium around the point B results in the following vertical forces:

$$\Delta F_{z,y}^{L} = -F_y \cdot \frac{h_g}{t}; \quad \Delta F_{z,y}^{R} = -\Delta F_{z,y}^{L} \tag{5}$$

Joining the contributions from Equations 3, 4 and 5, the dynamic variation of vertical forces follows:

$$\{\Delta F_z\} = \frac{1}{2} \cdot [\Delta F_{z,x}^{F} + \Delta F_{z,y}^{L};\ \Delta F_{z,x}^{F} + \Delta F_{z,y}^{R};\ \Delta F_{z,x}^{R} + \Delta F_{z,y}^{L};\ \Delta F_{z,x}^{R} + \Delta F_{z,y}^{R}] + \frac{F_z}{4} \tag{6}$$

The static forces are:

$$\{F_{z,static}\} = \frac{M \cdot g}{2} \cdot [w_d;\ w_d;\ (1 - w_d);\ (1 - w_d)] \tag{7}$$

where w_d is the weight distribution between front and rear, defined as:

$$w_d = \frac{M_F}{M} = 46\%$$

The final values of vertical forces are given by the summation of the static values with the dynamic variations and the aerodynamic downforce, computed as:

$$\{F_{z,downforce}\} = \frac{1}{2} \cdot \rho \cdot C_z \cdot S \cdot V_x^2 \tag{8}$$

with the vehicle parameters defined in Table 1.
Combining Equations from 6, 7, and 8 the resulting vertical load vector is:

$$\{F_z\} = \{F_{z,static}\} + \{\Delta F_z\} + \{F_{z,downforce}\} \tag{9}$$

The Simulink integration of Equations from 4 to 9 is shown below:

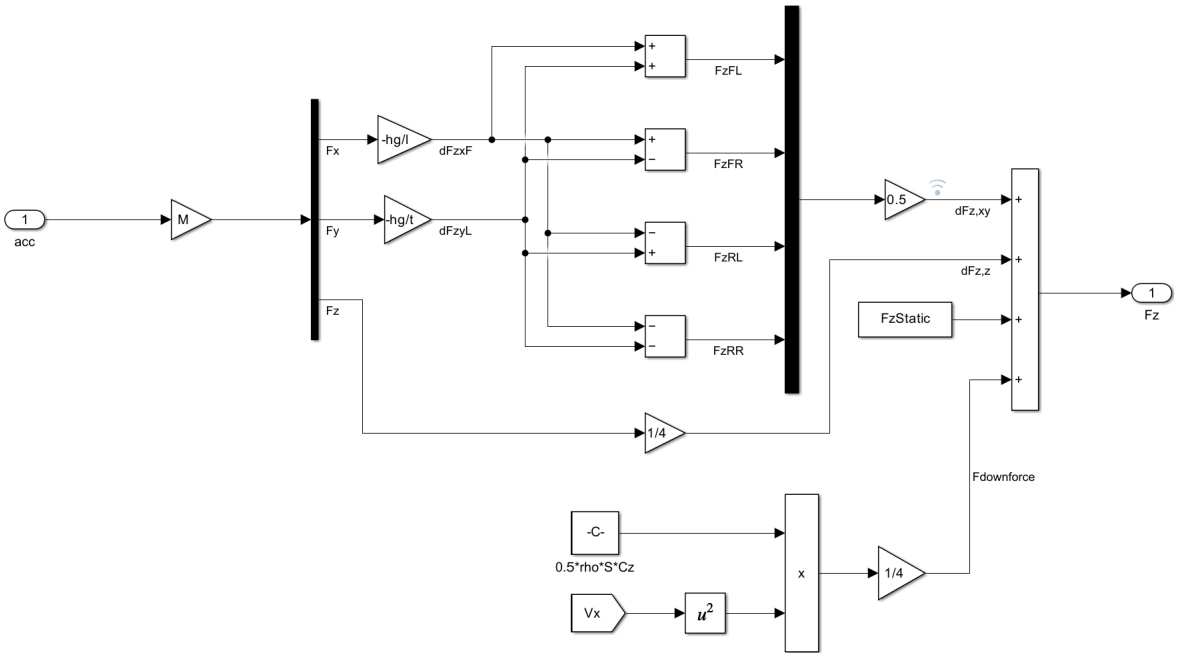

Figure 8: *Vertical forces computation.*

4. Relevant signals collection

Apart from the values introduced so far, other ones are relevant for the Control System and need to be collected:

- vehicle longitudinal speed (V_x): measured by an observer or by a non-contact optical speed sensor in a real scenario, or retrieved by vehicle simulation;
- vehicle yaw rate (ω_ψ): measured by the IMU in a real scenario, or retrieved by vehicle simulation;
- minimum torque limit (T_{MIN}): since this version of the TV is meant to operate only during traction, T_{MIN} is currently set to 0. In a future work, it could be set negative as well, to allow for bobcat mode (electric motors braking the wheels) or for the electric active braking system (eABS);
- maximum torque limit (T_{MAX}): this value is determined by a previous cascade of controls: Power Limit Control, Energy Efficient Control and Traction Control. Their traction is not a topic of this study, therefore T_{MAX} is just assumed to be an input.

Now that all the signals to be collected have been introduced, it is possible to step into the actual Control System part.

5. Upper Level Control

The ULC controls the magnitude of rotation of the vehicle. Its output corresponds to a yaw moment (Mz).
The logic behind the determination of the controlled yaw moment strongly affects the vehicle response and handling. The design of two different logics and the choice of the controller to actuate the control are extensively discussed in Section 5.

6. Lower Level Control

Receiving the yaw moment demand from the ULC, the LLC is the subsystem dealing with its actuation. Allocating torques on the four independent wheels is the way to deliver the target M_z. A wide range of possibilities is present to design this allocation algorithm, but two different ones, with different performances, are introduced in Section 6.

7. Vehicle system

In a real scenario, the final torque values are directly provided to the electric motor Control System. Instead, in a simulation environment, these values are converted into forces at wheel level and then, together with the steering angles, they are provided to a vehicle model that updates all the states exploited in the simulation loop. For a deeper explanation of the adopted vehicle model, look at Section 8.3.

Now that the TV flow has been introduced in detail, it is possible to move on with the presentation of the current state of the art of the TV control system and its design.

4 Literature overview

Recent research studies on the design of innovative Torque Vectoring control systems mainly focus on the design of alternative controllers for the ULC, while implementing standard and basic logics for the torque allocation.
Most of the studies share the same ULC flow: definition of a reference signal for the yaw rate (and possibly vehicle side-slip angle), calculation of the error with respect to the current state, stabilization of the error by means of an innovative control strategy. The strategies that have proven to be the most relevant and promising ones are:

- Optimal controller Linear–quadratic regulator (LQR) combined with a dynamic component that relies on a term identified as the yaw index [2], [3]. The LQR computes the optimal control input by minimizing the energy of the system states and the control input itself;
- Second order sliding mode controller (SOSM) [4], [5]: the system state is forced to evolve according a predefined set trajectory, significantly improving the system stability;
- Proportional integral derivative (PID) controller combined with an integral sliding mode (ISM) controller [6]: the continuous part of the state error, related to the system evolution, is controlled by the PID controller, while the discontinuous part, related to external disturbances of the system, is controlled by the ISM.

The model-based controllers, such as the LQR, lead to a more stable system evolution and enhanced performance; however, designing an accurate and reliable model can be challenging. Especially in Formula Student, where the funds are quite limited, undertaking accurate tests is relatively rare.
The SOSM controller, instead, has proven to lead to an improvement in control performance; however, the difficulty of integration represents a significant drawback.
A good trade-off between the complexity of integration and performance is the PID controller combined with an ISM. In the following Section 5.2, its implementation is discussed in detail.
Another noteworthy study [7] focuses on the control of the vehicle by means of stabilizing the yaw index (a parameter introduced later in Section 8.2). This alternative could be interesting for future work.

5 Design of the Upper Level Control

The choice of the logic for the ULC strongly affects the vehicle response and handling. Two concepts are presented in the following Sections: one very simple to implement and to tune but primitive and therefore not very common, and another one more oriented on the vehicle handling optimization, still keeping an easy integration, known as Direct Yaw Control (DYC).
As highlighted in the previous Section, the choice of the controller is crucial to guarantee stability and performance to the system.

5.1 Steering wheel based control

The steering wheel angle is directly related to the vehicle rotation: the more the driver steers, the more he wants the vehicle to rotate while cornering in a specific direction. As explained in Section 3.2, M_z is an equivalent control input for the vehicle, imposing its magnitude of rotation. Thus, it is reasonable to directly link its effect to that of the steering wheel angle.
It is straightforward to introduce a simple PID controller, with only the proportional term, to undertake this job. Considering the target yaw moment to reach $990N \cdot m$ (Section 3.1), the idea is to provide a yaw moment $1000N \cdot m$ when the driver steers 90°, which is almost the maximum steering wheel angle available.

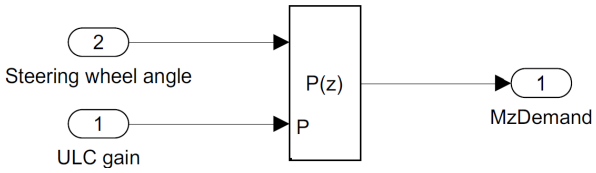

Figure 9: *Steering wheel based control.*

Since this gain value is based on a preliminary set target, it is merely provisional; a track testing session is needed to calibrate it.
To conclude, this control strategy is very simple to implement and is independent of vehicle state measurements, making it reliable.
A more interesting idea is to make this controller active and dependent on the speed. It is reasonable to suppose that the control has to be more aggressive at low speeds, but less invasive at high speeds, for safety reasons. The P gain would be retrieved by consulting a LUT previously built offline. The LUT can be defined in a simulation environment by means of an optimization process, where different P values are tested for each speed level, and the one leading to optimal handling results is selected.

An illustration of how this active control can be implemented in Simulink is shown below:

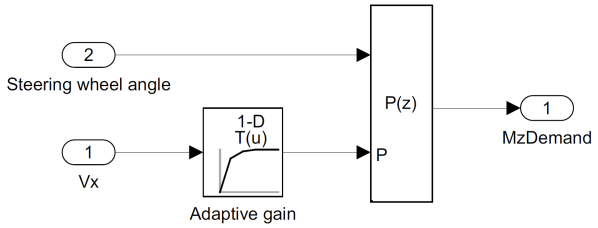

Figure 10: *Steering wheel based adaptive control.*

5.2 Direct Yaw moment Control

The DYC flow begins with the evaluation of a reference yaw rate signal, starting from the current vehicle states. It goes on with the computation of the error with respect to the current state. Then, the error is handled by a controller.

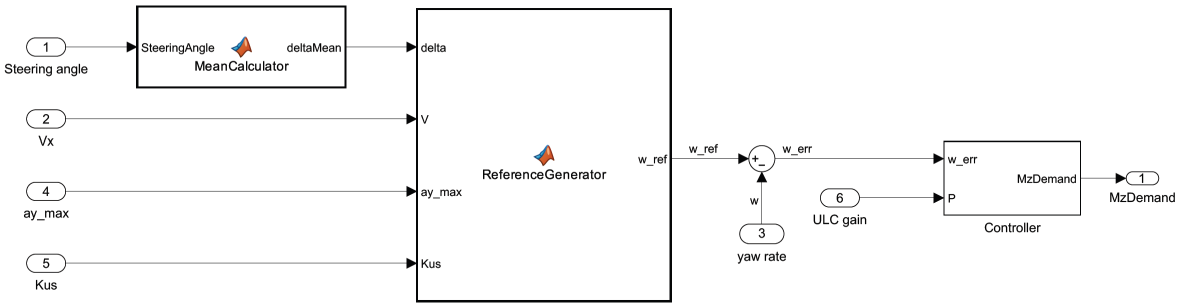

Figure 11: *DYC flow.*

As anticipated in the previous Section, the steering wheel angle (δ_{SW}) is directly related to the vehicle rotation. A vehicle state directly related to the rotation is the yaw rate (ω_ψ). Therefore, it is reasonable to define a function of the yaw rate dependent on the steering wheel angle [8].

The reference function is characterized by an initial linear part that saturates after a δ_{SW} threshold:

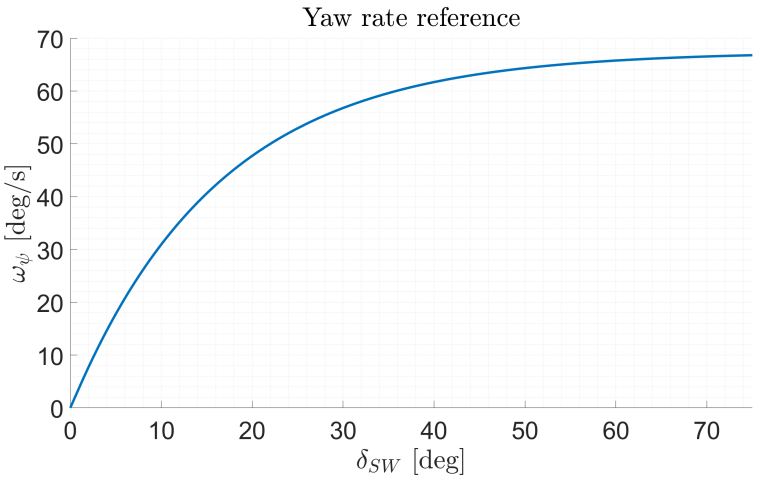

Figure 12: *Example of reference yaw rate trajectory.*

Despite the independent variable shown in the figure being the steering wheel angle δ_{SW}, the function adopts the steering angle at tire level δ as the independent variable. A simple conversion accounting for the steering assembly ratio is undertaken to move between the two values.

The starting point to define the linear part is the vehicle equation of motion, under the assumption of circular driving at steady-state. This is a reasonable approximation when considering a portion of a transient while cornering. The resulting equation follows:

$$\omega_\psi = \frac{V_x}{l + K_{US} \cdot V_x^2} \cdot \delta \tag{10}$$

where V_x is the longitudinal speed, l is the wheelbase and K_{US} is the under-steering coefficient, set as baseline $K_{US} = 0.3 \cdot 10^{-3}\ rad/(m/s^2)$, and defined as:

$$K_{US} = \frac{m}{l} \cdot \left(\frac{l_R}{C_F} - \frac{l_F}{C_R} \right) \tag{11}$$

where m is the vehicle mass, C_F and C_R are the front and rear cornering stiffness, l_F and l_R are the front and rear axle distances with respect to the center of gravity (COG).

From now on, the coefficient multiplying the steering angle in Equation 10 is identified as α:

$$\alpha = \frac{V_x}{l + K_{US} \cdot V_x^2} \tag{12}$$

Moving to the steering angle saturation point, instead, it is associated with the lateral acceleration value which tracks the transition from the approximately linear behavior

of the vehicle to the saturation:

$$\delta^* = K_{US} \cdot a_y^* \tag{13}$$

where the lateral acceleration transition value is reasonably set to $a_y^* = 0.65 \cdot a_y^{MAX}$. The maximum lateral acceleration can be evaluated by undertaking a circular driving maneuver at increasing speed. The value at which the driver loses control of the vehicle is a_y^{MAX}. Before undertaking the test, the baseline is $a_y^{MAX} = 2.5g$. This value is also used to calculate which is the maximum yaw rate reachable at saturation:

$$\omega_\psi^{MAX} = \frac{a_y^{MAX}}{V_x} \tag{14}$$

The yaw rate value corresponding to the transition point is:

$$\omega_\psi^* = \frac{V_x}{l + K_{US} \cdot V_x^2} \cdot \delta^* \tag{15}$$

Starting from all these parameters just introduced, the saturation region function is defined as:

$$\omega_\psi = \omega_\psi^{MAX} + \left(\omega_\psi^* - \omega_\psi^{MAX}\right) \cdot e^{\frac{\alpha \cdot (\delta - \delta^*)}{\omega_\psi^* - \omega_\psi^{MAX}}} \tag{16}$$

To summarize the piece-wise equation making up the yaw rate reference shown in Figure 12:

$$\omega_\psi = \begin{cases} \frac{V_x}{l + K_{US} \cdot V_x^2} \cdot \delta, & \delta \leq \delta^* \\ \omega_\psi^{MAX} + \left(\omega_\psi^* - \omega_\psi^{MAX}\right) \cdot e^{\frac{\alpha \cdot (\delta - \delta^*)}{\omega_\psi^* - \omega_\psi^{MAX}}}, & \delta > \delta^* \end{cases} \tag{17}$$

where the input states coming from the CAN bus are the vehicle longitudinal speed (V_x) and the two steering angles of the front wheels, used to evaluate the single mean value δ: $\delta = \frac{\delta_L + \delta_R}{2}$; the parameters to be tuned, instead, are the maximum lateral acceleration a_y^{MAX} and the under-steering coefficient K_{US}.

A sensitivity analysis is undertaken to show how much each of these two parameters influences the reference generation:

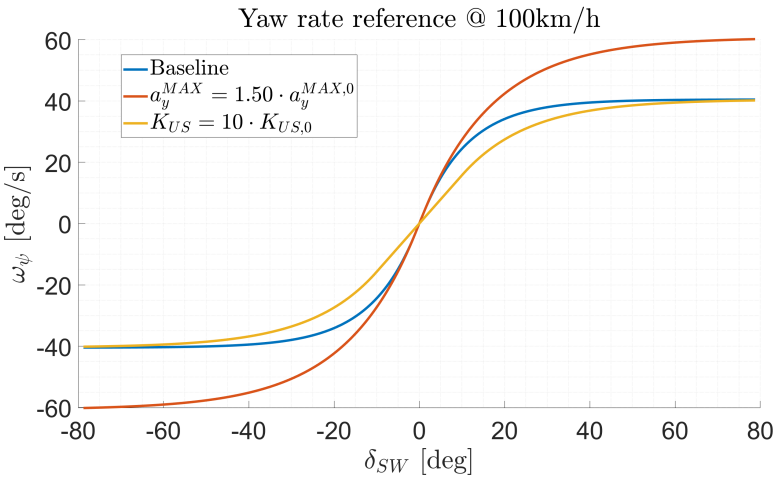

Figure 13: *Yaw rate reference parameters sensitivity.*

In a future work, the yaw rate control could be matched with the vehicle side slip angle (β) control to further enhance the handling performance. The accurate computation of this last vehicle state is very complex, and it is part of the second part of this thesis project. Therefore, the implementation of this control section is not treated in this work.

Once the reference signal is compared with the current state, the error is handled by the controller. For this application, as anticipated in Section 4, a PID controller with Integral Sliding Mode (ISM) control is implemented.
To make the process easier and more effective, the design and validation of this control strategy are split into two steps: PID controller implementation first, and then ISM control implementation. This decision finds a reason when considering the purpose of the controllers themselves. As anticipated in Section 4, the PID addresses the continuous part of the error which is related to the regular evolution of vehicle states, while the ISM deals with the discontinuous part generated by external disturbances acting on the vehicle to increase the system robustness. Therefore, it is more easy to calibrate the standard controller first, and then the complementary one.
The PID controller is a pretty basic control strategy, made up of three terms (plus a supplementary one) handling the error in different ways:

- proportional term (P): it aims to attenuate the state error relative to current time instant;
- integral term (I): it aims to reduce the residual steady-state error. Therefore, it

acts on the past action of the controller;

- derivative term (D): observing the derivative of the error, it tracks its evolution during the time, controlling it in advance;
- filter for the derivative term (τ): the derivative term can lead to some oscillations in the control input activity, that can be attenuated by a low-pass filter. Moreover, the transfer function must have the degree of the numerator minor or equal to the degree of the denominator to be proper. This filter term, therefore, is also implemented to satisfy this condition.

The transfer function taking as input the error and giving back the control input, representative of the PID controller, is:

$$G_{PID} = P + \frac{I}{s} + \frac{D \cdot s}{1 + \tau \cdot s} \tag{18}$$

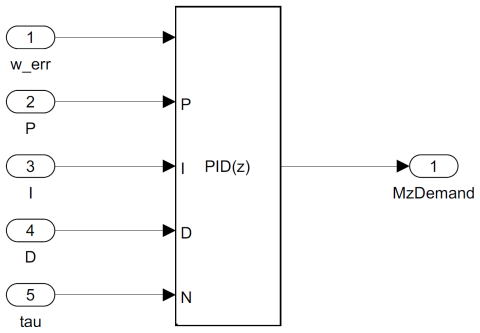

Figure 14: *DYC - PID controller.*

Concerning the implementation of the ISM, the basic idea is to force the system state evolution to follow a specific trajectory, called the sliding manifold.

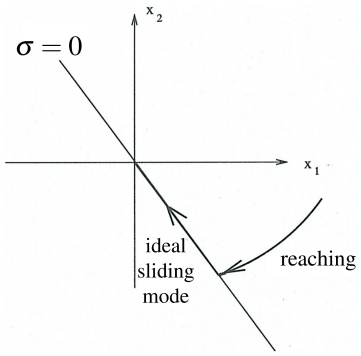

Figure 15: *Ideal sliding mode operation [9].*

To do so, a sliding surface (s) is defined representing the discontinuities of the error due to uncertainties and external disturbances. It is the combination of the overall yaw

rate error (s_0) with its continuous compensating part (z):

$$s = s_0 - z \tag{19}$$

To enforce integral sliding, the system is designed to start and to stay on the sliding manifold. Therefore, the following two conditions are imposed:

$$\begin{cases} s(0) = 0 \implies z(0) = s_0(\omega_{\psi,\ err}(0)) \\ \dot{s}(t) = 0 \implies \dot{z} = \dot{s}_0 \end{cases} \tag{20}$$

Developing the derivative of s_0 with respect to the time, according to the chain rule:

$$\dot{s}_0 = \frac{ds_0}{d\omega_{\psi,\ err}} \cdot \frac{d\omega_{\psi,\ err}}{dt} = \frac{ds_0}{d\omega_{\psi,\ err}} \cdot (\dot{\omega}_{\psi,\ ref} - \dot{\omega}_{\psi}) \tag{21}$$

The first derivative term is neglected: since s_0 is the overall yaw rate, the derivative with respect to itself turns out to be 1.
In the case of the compensating term z, the intended current yaw acceleration is not the overall value, but its continuous part:

$$\dot{z} = \dot{\omega}_{\psi,\ ref} - \hat{\dot{\omega}}_{\psi} \tag{22}$$

The idea to isolate this part is to subtract the demanded overall yaw moment $M_{z,\ ISM}$ with the one demanded by the sliding mode $M_{z,\ SM}$, accounting for the disturbance. Then, knowing the yaw moment of inertia: $\hat{\dot{\omega}}_{\psi} = \frac{1}{J_z} \cdot (M_{z,\ ISM} - M_{z,\ SM})$.
Thus, the final formulation of the derivative of the compensating term is:

$$\dot{z} = \dot{\omega}_{\psi,\ ref} - \frac{1}{J_z} \cdot (M_{z,\ ISM} - M_{z,\ SM}) \tag{23}$$

Now that it is clear how the sliding surface is designed, a control action based on its sign is determined, according to the tunable parameter K_{SM}. A low-pass filter is applied afterwards to prevent the phenomenon of chattering: high-frequency oscillations of the controlled variable.

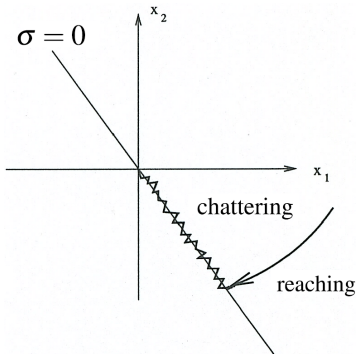

Figure 16: *Real sliding mode operation [9].*

The goal is to satisfy the η-reaching condition, stating that the sliding surface is being driven toward zero with a guaranteed minimum rate:

$$s \cdot \dot{s} < -\eta \cdot |s| \tag{24}$$

This condition guarantees stability and robustness for the system.
Finally, the implementation of this control structure is shown:

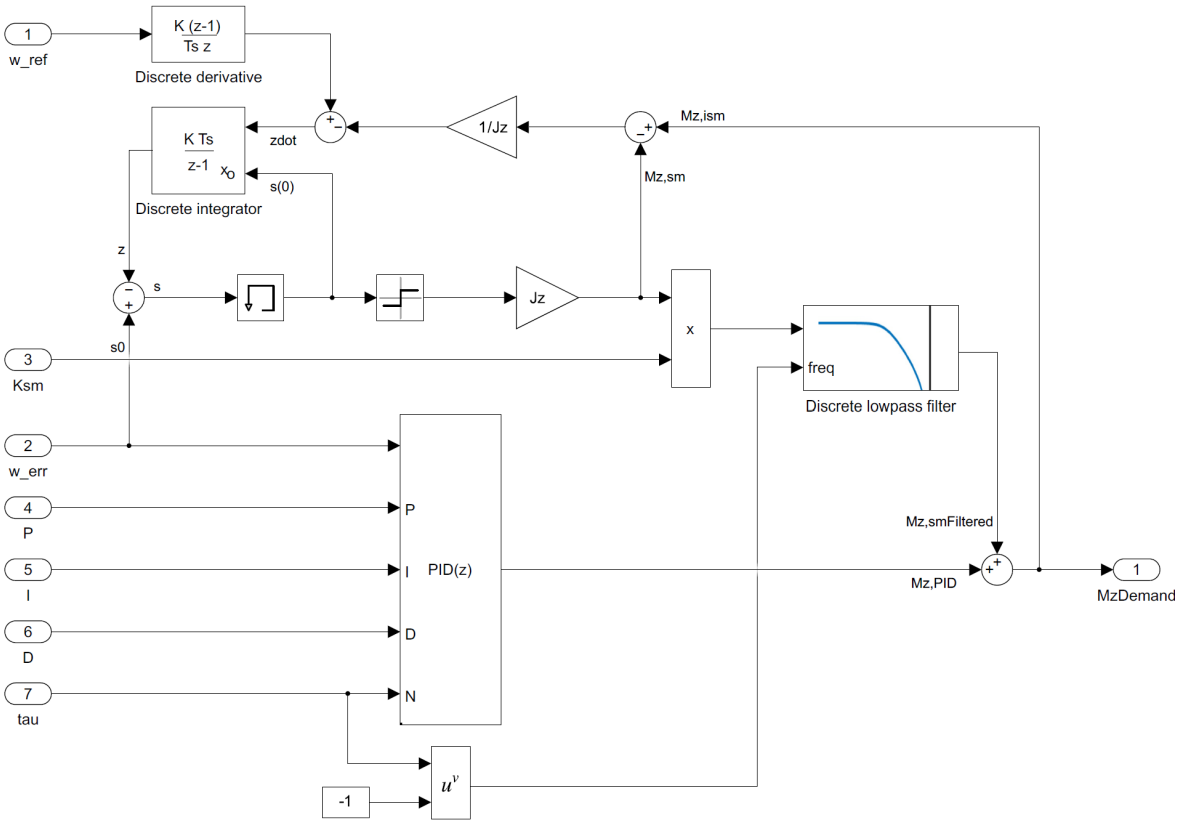

Figure 17: *DYC - PID with ISM controller.*

6 Design of the Lower Level Control

As for the ULC, two different algorithms are developed for the LLC: one is rule-based, pretty light from the computational point of view, but less accurate when it comes to constraints to respect and criteria to satisfy; the other one is based on an optimization problem, introducing an easy interface with the external constraints and input, but a more complex set-up and a heavier computational demand.
Both algorithms are based on the same target: arrange the torque on the two lateral sides of the vehicle to satisfy the yaw moment demand from the ULC and simultaneously, on each lateral side, to keep the ratio of the front torque with respect to the rear as close as possible to the front-to-rear vertical force ratio.
The two levels share the same six inputs and single output (final torque values to be delivered by the EMs). The inputs are the following:

- throttle pedal (h_a $[p.u.]$);
- vertical force (F_z $[N]$) on the four wheels;
- minimum torque limit (T_{MIN} $[Nm]$);
- maximum torque limit (T_{MAX} $[Nm]$);
- demanded yaw moment (M_z $[Nm]$);
- steering angle (δ $[rad]$) at wheel level, both for the left and right wheels.

6.1 Rule-based control

For ease of operation, this torque allocation algorithm deals with forces, eventually converted into torques. Its flow is split into four main steps:

- preliminary distribution of the forces for each lateral side (left and right). The logic is simple: the same quantity of force is added to one side and subtracted to the other one, in order to deploy the demanded yaw moment. A preliminary recovery of the residual yaw moment is undertaken;
- check of the preliminary set forces for each lateral side to verify if they respect the force bounds. If the saturation is reached on one side (upper or lower bound), the force is recovered on the other one;
- longitudinal distribution of the forces (front to rear), accounting for the saturation of the torque limits. The distribution follows the principle introduced in the

previous Section 6: $\frac{T_{F(L/R)}}{T_{R(L/R)}} = \frac{F_{z,\ F(L/R)}}{F_{z,\ R(L/R)}}$. A final recovery of the residual yaw moment is effectuated, by means of the rear axle;

- conversion of the final force values into torques.

The complete algorithm of this strategy is detailed in the Appendix A.

6.2 Optimal control

Developing a robust algorithm for the torque allocation is a tricky task to carry out, since different constraints must be satisfied and the target yaw moment must be accurately delivered. An effective solution to deal with these tight requirements is the setup of an optimization problem.
This problem consists in finding the optimal solution that minimizes a defined cost function. According to how the cost function is defined, an adapt solver has to be set up.
The states to be optimized are the torques for each wheel:

$$\eta = [T_{FL};\ T_{FR};\ T_{RL};\ T_{RR}] \tag{25}$$

The basic idea is that the more a tire is vertically loaded, the more it is able to deliver longitudinal force (without considering saturation due to vertical force). To exploit this principle, it is desired that for the two wheels on each side the ratio of their assigned torques is kept as close as possible to the ratio between the front and the rear vertical loads, meaning that the difference between the two ratios has to be minimized. Moreover, the control is allowed to diminish the delivered torque (within a limit), with respect to the one requested by the driver, aiming to satisfy the demanded yaw moment.
Starting from these requirements, the cost function is defined as:

$$J(\eta) = \left(\frac{T_{FL}}{T_{RL}} - \frac{F_{zFL}}{F_{zRL}}\right)^2 + \left(\frac{T_{FR}}{T_{RR}} - \frac{F_{zFR}}{F_{zRR}}\right)^2 + \gamma \cdot (\sum_{i=1}^{4} T_i - T_{demand})^2 \tag{26}$$

where the third term presents a gain γ, introduced to penalize the decrease of torque when the demanded yaw moment is low. In other terms, a low demanded yaw moment corresponds to a lower overall control effect from the LLC. Indeed, the gain is defined as:

$$\gamma = \begin{cases} \frac{\gamma_0}{M_z} & M_z > \epsilon \\ \frac{\gamma_0}{\epsilon} & M_z < \epsilon \end{cases}, \quad with\ \epsilon = 3N \cdot m,\ \gamma_0 = 500N \cdot m \tag{27}$$

To avoid mathematical issues related to the divisions, Equation 26 is rearranged presenting only multiplications:

$$J(\eta) = (F_{zRL} \cdot T_{FL} - F_{zFL} \cdot T_{RL})^2 + (F_{zRR} \cdot T_{FR} - F_{zFR} \cdot T_{RR})^2 + \gamma \cdot (\sum_{i=1}^{4} T_i - T_{demand})^2 \quad (28)$$

The squares are introduced to make this cost function quadratic, and so to ensure a minimum to the optimization problem. Therefore, this problem is a Quadratic Programming (QP). `MATLAB` defines QP as "the mathematical problem of finding a vector x that minimizes a quadratic function" [10]. This function is typically written in the form:

$$J(\eta) = \frac{1}{2} \cdot \eta^\top \cdot H \cdot \eta + f^\top \cdot \eta \quad (29)$$

where H is the Hessian matrix and f is the gradient:

$$f = \nabla J(T) = \begin{bmatrix} \frac{\partial J}{\partial \eta_1} & \dots & \frac{\partial J}{\partial \eta_4} \end{bmatrix}^\top \quad (30)$$

$$H = \begin{bmatrix} \frac{\partial^2 J}{\partial \eta_1^2} & \dots & \frac{\partial^2 J}{\partial \eta_1 \partial \eta_4} \\ \vdots & \ddots & \vdots \\ \frac{\partial^2 J}{\partial \eta_4 \partial \eta_1} & \dots & \frac{\partial^2 J}{\partial \eta_4^2} \end{bmatrix} \quad (31)$$

Two methods can be introduced to compute the Hessian and the gradient:

- A numerical approach: more simple, but less precise, with the possibility to lead to numerical errors;
- An algebraic approach: more stable and accurate.

According to the numerical approach, the computation is carried out around a generic point $\eta = [0;\ 0;\ 0;\ 0]$. To do so, the difference quotient is used:

$$f = \begin{bmatrix} \frac{J(\eta_1 + dT,\ \eta_2,\ \eta_3,\ \eta_4)}{dT} & \dots & \frac{J(\eta_1,\ \eta_2,\ \eta_3,\ \eta_4 + dT)}{dT} \end{bmatrix}^T \quad (32)$$

```
% Cost function defintion:
J = @(T) (Fz(3)*T(1) - Fz(1)*T(3))^2 + ...
         (Fz(4)*T(2) - Fz(2)*T(4))^2 + ...
         gamma*((T(1) + T(2) + T(3) + T(4)) - trqDemand)^2;

% Numerical computation of the cost function gradient:
T0 = zeros(4,1); % Generic point within the cost function domain
dT = 1e-5;       % Small step for finite difference
f = zeros(4,1);  % Gradient initialization
for i = 1:4
```

```
    Tincremental = T0;
    Tincremental(i) = Tincremental(i) + dT;
    f(i) = (J(Tincremental) - J(T0)) / dT;
end
```

Concerning the Hessian matrix terms, the difference quotient is applied twice for their computation:

$$\frac{\partial^2 J}{\partial \eta_i \partial \eta_j} \approx \frac{J(\eta_i + dT, \eta_j + dT) - J(\eta_i + dT, \eta_j) - J(\eta_i, \eta_j + dT) + J(\eta_i, \eta_j)}{dT^2} \tag{33}$$

```
% Numerical computation of the cost function Hessian matrix:
H = zeros(4,4); % Hessian matrix initialization
for i = 1:4
    for j = 1:4
        Tincremental1 = T0; Tincremental2 = T0; Tincremental3 =
            T0;
        Tincremental1(i) = Tincremental1(i) + dT;
        Tincremental1(j) = Tincremental1(j) + dT;
        Tincremental2(i) = Tincremental2(i) + dT;
        Tincremental3(j) = Tincremental3(j) + dT;
        H(i,j) = (J(Tincremental1) - J(Tincremental2) -
            J(Tincremental3) + J(T0)) / dT^2;
    end
end
```

Concerning the algebraic approach, instead, the property of the matricial multiplication is exploited to rebuild the target cost function.
Three vectors Q are defined:

$$Q_1 = [Fz(3),\ 0,\ -Fz(1),\ 0] \tag{34}$$

$$Q_2 = [0,\ Fz(4),\ 0,\ -Fz(2)] \tag{35}$$

$$Q_3 = \sqrt{\gamma} \cdot [1,\ 1,\ 1,\ 1] \tag{36}$$

The Hessian Matrix is rebuilt by multiplying each vector times its transpose and summing all the resulting terms:

$$H = Q_1^\top \cdot Q_1 + Q_2^\top \cdot Q_2 + Q_3^\top \cdot Q_3 \tag{37}$$

Its goal is to bring all the second-degree and mixed terms inside the cost function. Instead, the gradient vector integrates all the first-degree terms:

$$f = -T_{demand} \cdot \gamma \cdot \begin{bmatrix} 1 \\ 1 \\ 1 \\ 1 \end{bmatrix} \tag{38}$$

Look at the Appendix B for the complete demonstration: from the Hessian matrix and the gradient vector to Equation 28.
Later on, in Section 7, the definition of the cost function is further expanded to satisfy some requirements imposed by the integrated solver.
If there is the possibility to set up a warm start set of values, in order to enhance the optimal point searching time, then this set is chosen:

$$T_{WS} = [1;\ 1;\ 1;\ 1] \cdot \frac{T_{demand}}{4} \tag{39}$$

An important possibility that the optimization problem offers is the integration of upper and lower limits for the states and the integration of constraint functions.
The upper limit is defined apriori by the Traction Control (TC), as well as the lower limit by the Electric Active Braking System (E-ABS) or by the maximum stress allowable on the gearbox. Since the traction control is still in a development phase, the upper torque limits correspond to the maximum deliverable torque from the EM. The braking scenario is not considered in this development phase and, mechanically wise, a conservative choice is taken for the gearbox, so the lower torque bounds are set equal to 0:

$$u_b = [1;\ 1;\ 1;\ 1] \cdot T_{EM}^{MAX} \tag{40}$$

$$l_b = [0;\ 0;\ 0;\ 0] \tag{41}$$

Two kinds of constraint functions can be typically defined:

- soft constraints: the states must be lower than a certain set of thresholds;
- hard constraints: the states must be equal to a certain set of values.

By imposing soft constraints, it is possible to avoid a situation where the delivered torque exceeds the torque demand, thereby violating the FS rules (Section 2), and to prevent the torque delivered from diminishing too much with respect to the demand, which impacts drivability. A maximum decrease in the 20% is allowed. To impose these constraints, a matrix form is exploited:

$$[A] \cdot \{\eta\} \leq \{b\} \tag{42}$$

where:

$$A = \begin{bmatrix} 1 & 1 & 1 & 1 \\ -1 & -1 & -1 & -1 \end{bmatrix}, \quad b = \begin{bmatrix} T_{demand} \\ -0.8 \cdot T_{demand} \end{bmatrix} \tag{43}$$

In the same way, but using hard constraints, it is imposed on the control to find a solution that guarantees the requested yaw moment:

$$[A_{eq}] \cdot \{\eta\} = \{b_{eq}\} \tag{44}$$

where:

$$A_{eq} = \begin{bmatrix} \left[-\frac{t}{2} \cdot cos(\delta_L) + l_f \cdot sin(\delta_L) \right] \cdot \frac{1}{\tau_{GB} \cdot R_l} \\ \left[\frac{t}{2} \cdot cos(\delta_R) + l_f \cdot sin(\delta_R) \right] \cdot \frac{1}{\tau_{GB} \cdot R_l} \\ -\frac{t/2}{\tau_{GB} \cdot R_l} \\ \frac{t/2}{\tau_{GB} \cdot R_l} \end{bmatrix}^T, \quad b_{eq} = \begin{bmatrix} M_z \end{bmatrix} \tag{45}$$

The A_{eq} matrix is retrieved by means of a free body diagram. According to the positive sign convention of the rotation around the vertical vehicle body axis, the equivalent yaw moment is evaluated. This equivalent moment is generated by the forces related to the torques deployed by each EM:

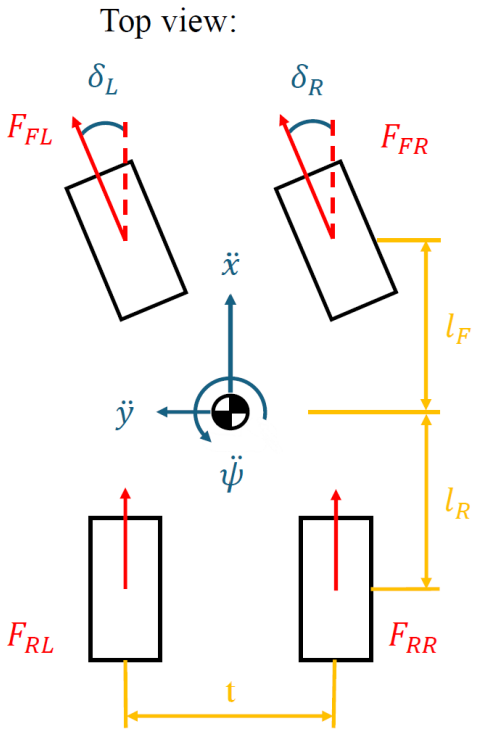

Figure 18: *Yaw moment free body diagram.*

The yaw moment equation follows:

$$M_z = -F_{FL} \cdot cos(\delta_L) \cdot \frac{t}{2} + F_{FL} \cdot sin(\delta_L) \cdot l_F + F_{FR} \cdot cos(\delta_R) \cdot \frac{t}{2} + F_{FR} \cdot sin(\delta_R) \cdot l_F - F_{RL} \cdot \frac{t}{2} + F_{RR} \cdot \frac{t}{2} \tag{46}$$

To convert the forces to torque values, the following relation is exploited:

$$F_i = \frac{T_i}{\tau_{GB} \cdot R_l} \tag{47}$$

where τ_{GB} is the gearbox ratio and R_l is the tire loaded radius.

Finally, when solving the optimization problem, it is reasonable to suppose that conditions in which the controlled yaw moment cannot be reached by the torque allocation can occur. In these conditions, the solver is intended to return an error code that is used to decrease the demanded yaw moment until the solver retrieves a feasible solution to the optimization problem. The implementation of this solution is highlighted in yellow color in Figure 19.
The complete architecture of the LLC with the optimal control logic follows:

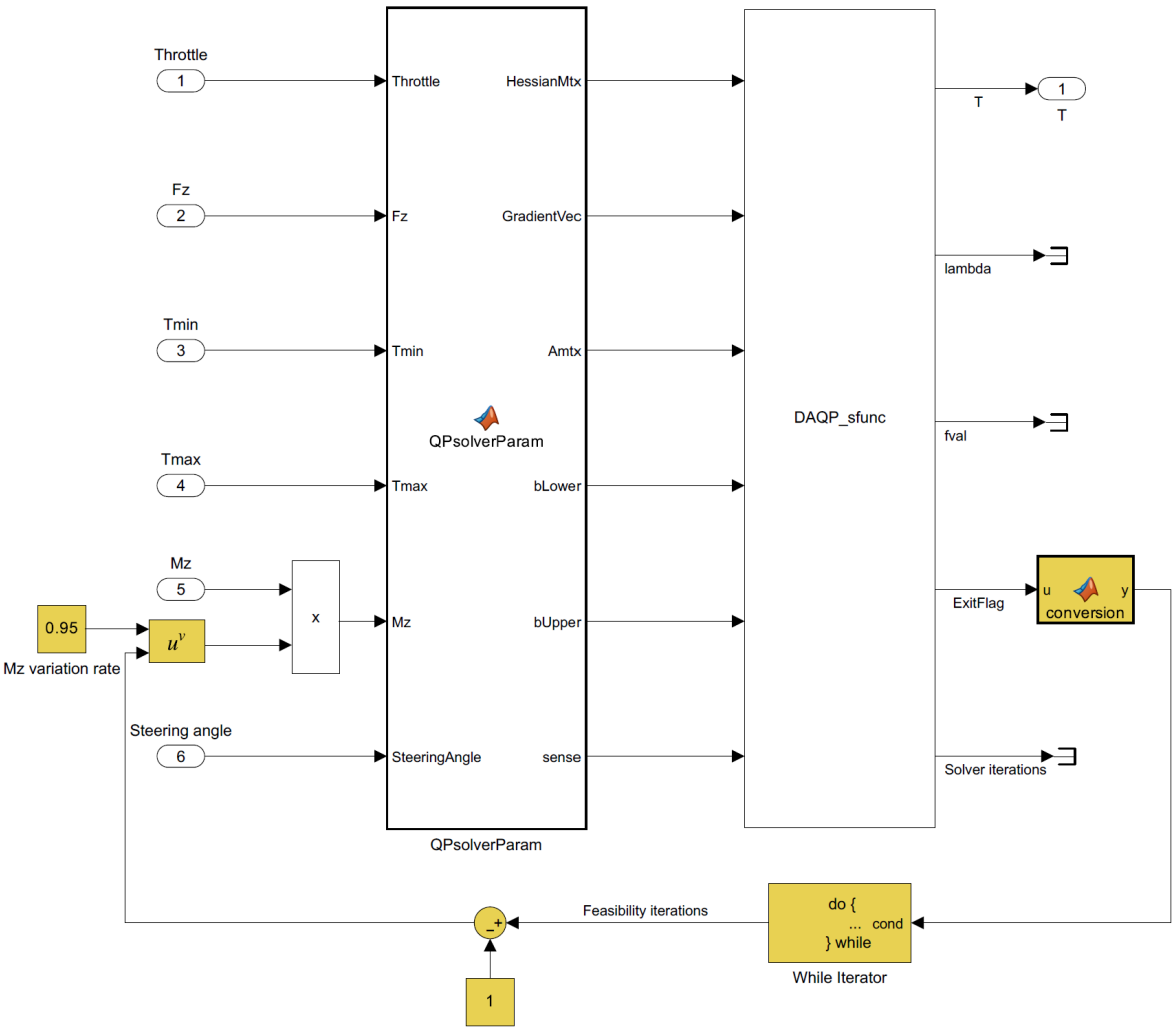

Figure 19: *LLC optimal control architecture.*

7 Integration

The integration of the Control System and its subsystems at software level has already been discussed in the previous Sections. The TV is developed entirely within the `MATLAB/Simulink` environment.
The next step is the integration of the Control System into the hardware. The target hardware is the Electronic Control Unit (ECU) dSpace® MicroAutoBox II.
In order to upload the software onto the ECU, a compilation procedure is carried out. It is characterized by the following steps:

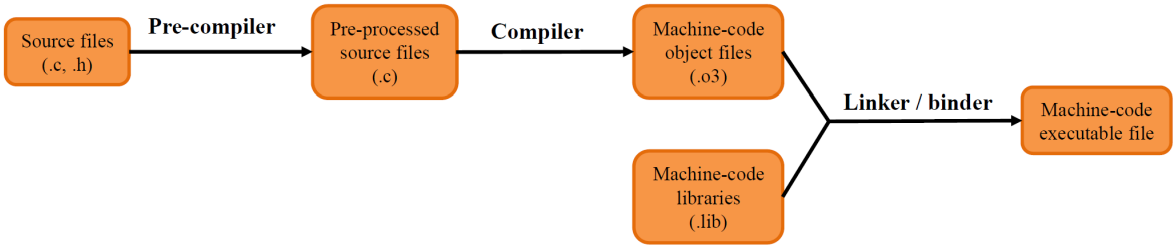

Figure 20: *Compilation process.*

During the conversion of the `MATLAB/Simulink` code into C-code, some of the most recent libraries from Matlab are not supported by the Matlab version running on the dSpace® MicroAutoBox II. An example is the built-in function `quadprog`, which is used for solving quadratic programming problems, such as the one introduced in Section 6.2.
Therefore, an alternative library to carry out the same task has been integrated. The DAQP S-function [11] has proven to provide an easy integration process and robust results during the validation phase.
Nevertheless, the formulation of the Hessian matrix, a subject of quadratic programming, requires an adjustment to comply with the requirements of the DAQP solver. Indeed, the solver operates correctly only with a positive definite Hessian matrix. To comply with this requirement and to avoid an alteration of the cost function that would compromise its scope, a redundant term is added, as anticipated in Section 6.2. This term represents the equality constraint relative to the requested yaw moment, which has already been imposed separately. It is implemented by means of the vector Q joint to the already present ones making up the Hessian matrix:

$$Q_4 = A_{eq} \tag{48}$$

The Hessian matrix formulation is modified accordingly:

$$H = Q_1^\top \cdot Q_1 + Q_2^\top \cdot Q_2 + Q_3^\top \cdot Q_3 + Q_4^\top \cdot Q_4 \tag{49}$$

To keep the cost function unaffected, the gradient vector is updated as well:

$$f = -T_{demand} \cdot \gamma \cdot \begin{bmatrix} 1 & 1 & 1 & 1 \end{bmatrix}^{\top} - M_z \cdot Q_4^{\top} \tag{50}$$

8 Project test

The goal of this process phase is:

- to verify that the Control System operates as intended (Section 2) within a simulation environment;
- to calibrate the controller to achieve optimal performance;
- to validate the Control System performance, by tracking relevant KPIs.

8.1 Test planning

For this phase of the control system development, different standard maneuvers are taken into account. This set of maneuvers is representative of different scenarios of lateral driving.

1. Slalom

The driver reaches a longitudinal speed of $30km/h$ while driving straight, then enters the slalom, effectuating 5 changes of direction. The throttle pedal is kept constant.

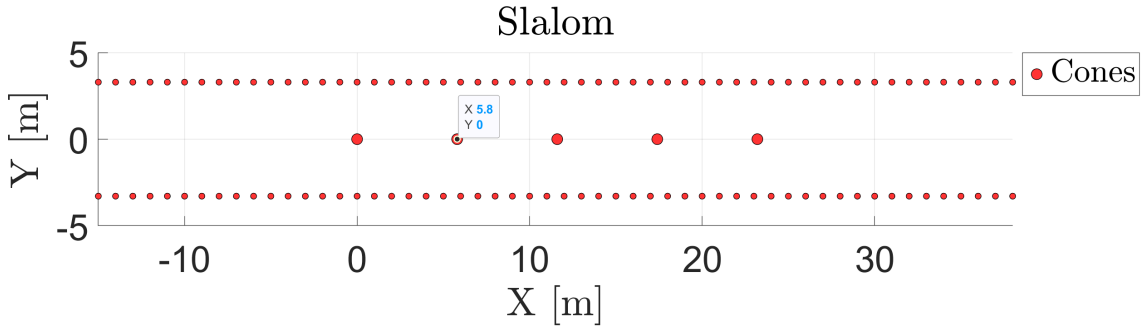

Figure 21: *Slalom maneuver.*

2. Double lane change

The driver reaches a longitudinal speed of $30km/h$ driving straight, then he undertakes a lane change twice at a constant throttle pedal position. Between the two lane changes, a straight part of $15m$ is present.

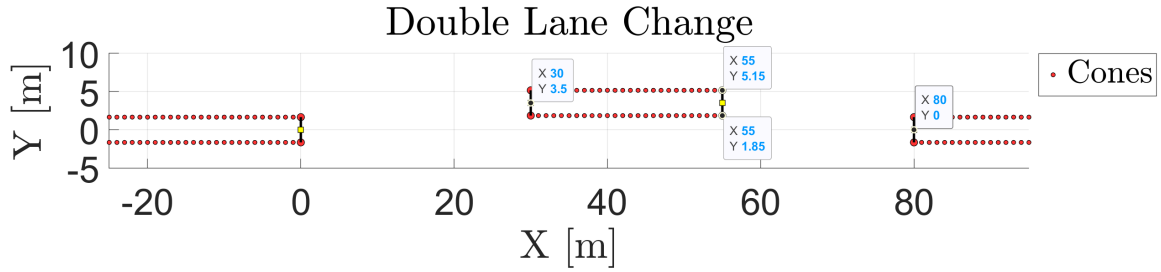

Figure 22: *Double lane change maneuver.*

3. Step steer

The driver reaches a longitudinal speed of $40km/h$ driving straight, and then he applies an instantaneous steering wheel angle input. Its value $\delta_{SW} = 90°$ is kept constant for about 7 seconds to allow the relevant vehicle states to stabilize. The throttle position is kept constant as well.

8.2 Definition of KPIs

The Key Performance Indicators (KPIs) allow to quantify the performance of the implemented control system. Therefore, they are crucial during the validation and especially the calibration phases. For this sake, seven fundamental parameters are introduced and used during the data analysis:

1. Maximum lateral acceleration

This value corresponds to the maximum during the maneuver:

$$a_y^{MAX} = max(a_y(t)) \tag{51}$$

To avoid that a misleading value, due to the noise of the data coming from the IMU, is taken, this maximum value trend must be regular for a minimum time $T_{measure} = 0.05s$.

2. Average steering wheel angle

To compute the average, the Root Mean Square (RMS) of the signal is evaluated. This is done to make the average independent of the sign of the steering wheel angle:

$$\delta_{SW}^{AVG} = rms(\delta_{SW}(t)) = \sqrt{\frac{1}{T_f - T_0}\int_{T_0}^{T_f}[\delta_{SW}(t)]^2 dt} \tag{52}$$

where T_0 and T_f are respectively the starting and final time instants of the maneuver.

3. Maximum trajectory error

This value corresponds to the maximum during the maneuver:

$$e_t^{MAX} = max(e_t(t)) \tag{53}$$

The trajectory error is the composition of the heading (e_h) and the lateral error (e_y). The heading error is defined as:

$$e_h = \psi - \psi^{R,\ c} \tag{54}$$

where ψ is the current yaw angle and $\psi^{R,\ c}$ is the reference yaw angle with respect to the trajectory point closest to the vehicle.
The lateral error, instead, is derived by integration of the following state:

$$\dot{e}_y = V_y + V_x \cdot e_h \tag{55}$$

Thus, the final equation of the trajectory error follows:

$$e_t = e_h + e_y \tag{56}$$

As in the previous cases, the maximum value trend must be regular for a minimum time $T_{measure} = 0.05s$.

4. Yaw rate damping

This KPI is specifically related to the step steer maneuver introduced in the previous Section. The step steering wheel input generates a yaw rate response. Of this signal, two parameters are evaluated according to the ISO ISO 7401:2011:

- response time; the origin for each response is the time at which the steering-wheel angle change is 50% complete. Response time is thus defined as the time, measured from this reference, for the vehicle transient response to first reach 90% of its new steady-state value;
- overshoot value; it is calculated as a ratio: the difference between peak value and steady-state value divided by the steady-state value.

5. Lateral acceleration response

Also in this case, the KPI is specifically related to the step steer maneuver. Continuing to adopt the ISO 7401:2011 definitions, the lateral acceleration response is the response time relative to the a_y signal.

6. Average yaw index

The yaw index is a KPI providing information about the current under-steering behavior of the vehicle [2]. It corresponds to the derivative of the vehicle side slip angle ($\dot{\beta}$), under the assumption of constant speed turn, with a small vehicle side slip angle (β) value.
To retrieve its value, the overall lateral acceleration of the vehicle is analyzed beforehand. It is made up of the derivative of the lateral speed and of the centripetal acceleration:

$$a_y = \dot{V}_y + \frac{V_x^2}{R} = \dot{V}_y + \omega_\psi \cdot V_x \tag{57}$$

Dividing this equation by the longitudinal speed V_x, the derivative of the vehicle side slip angle is retrieved:

$$I_\psi = \dot{\beta} = \frac{a_y}{V_x} - \omega_\psi \tag{58}$$

When the vehicle experiences a decrease of vehicle side slip during the middle phase of the corner, the vehicle behavior is under-steering; instead, it's over-steering for an increase of β. Figure 23 is representative of this behavior:

- condition a corresponds to a neutral-steering condition;
- condition b corresponds to an over-steering condition;
- condition c corresponds to an under-steering condition.

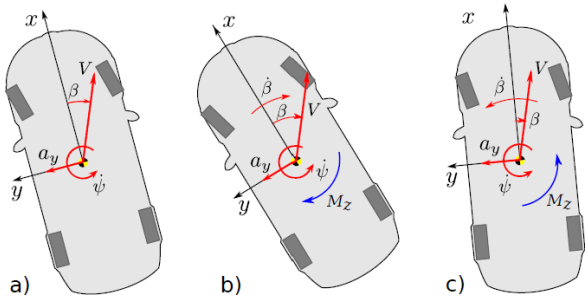

Figure 23: *Yaw index behavior to the vehicle under-steering behavior.*

Therefore, negative values of I_ψ correspond to an under-steering vehicle, while positive values correspond to an over-steering vehicle.
As done for the average steering wheel angle, the root mean square value is also adopted as the final indicator of the average yaw index value:

$$I_\psi^{AVG} = rms(I_\psi(t)) = \sqrt{\frac{1}{T_f - T_0}\int_{T_0}^{T_f} [I_\psi(t)]^2 dt} \tag{59}$$

8.3 Simulation

The vehicle model adopted for the simulation of the torque vectoring is a 3 DOFs dual track model. The longitudinal speed is constant during the simulation; thus, the equations of motion are relative to the lateral and rotational (yaw) degrees of freedom of the vehicle:

$$a_y = \frac{1}{M} \cdot (F_y^{FL} \cdot cos(\delta_L) + F_y^{FR} \cdot cos(\delta_R) + F_y^{FL} + F_y^{RR}) \tag{60}$$

$$\ddot{\psi} = \frac{1}{J_z} \cdot (F_y^{FL} \cdot cos(\delta_L) \cdot l_f + F_y^{FR} \cdot cos(\delta_R) \cdot l_f - F_y^{RL} \cdot l_r - F_y^{RR} \cdot l_r) + M_z \tag{61}$$

where M_z is the yaw moment contribution deployed by the TV.
The lateral tire model of the vehicle is built around experimental data collected from track testing sessions. It consists of a quadratic function for the cornering stiffness (C_α), with the vertical force as the independent variable:

$$C_\alpha = -15.2 \cdot 10^{-3} \cdot F_z^2 + 38 \cdot F_z \tag{62}$$

The lateral force is computed accordingly:

$$F_y = -C_\alpha(F_z) \cdot \alpha \tag{63}$$

where α is the side-slip angle of the tire. The accuracy of this formulation holds for small side-slip angle values.

The driver model adopted for the simulation is a PID controller with anti-windup, aiming to stabilize the current heading (e_h) and lateral (e_y) errors of the vehicle, with respect to the reference trajectory. Its goal is to determine the steering wheel angle command to the vehicle.

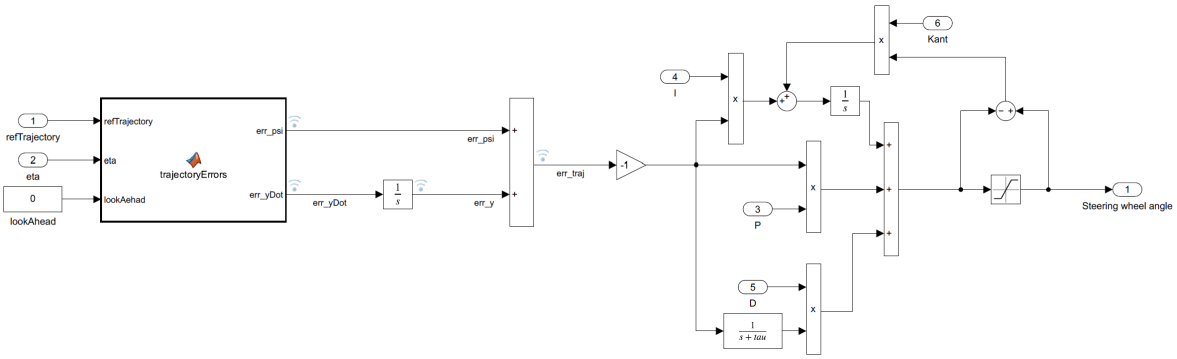

Figure 24: *Driver model architecture.*

8.4 Verification

The verification phase is undertaken by means of a slalom maneuver at a longitudinal speed $V_x = 20km/h$. The ULC logic adopted is the DYC, with only the P part active on the controller side. The LLC logics are rule-based and optimal control.
The parameters tracked during the maneuver are:

- yaw rate error (ω_ψ^{err}): the control system must follow the reference generated;
- yaw moment delivered by the TV: the LLC must deploy the yaw moment requested by the ULC;
- residues of the LLC target (LLC_{res}): the residues must be small to satisfy the goal of the LLC introduced in Section 6.

where $LLC_{res} = \left[\left(\frac{T_{FL}}{T_{RL}} - \frac{F_{zFL}}{F_{zRL}}\right)/\frac{F_{zFL}}{F_{zRL}} \cdot 100 + \left(\frac{T_{FR}}{T_{RR}} - \frac{F_{zFR}}{F_{zRR}}\right)/\frac{F_{zFR}}{F_{zRR}} \cdot 100\right]/2$. The results of the validation process follow:

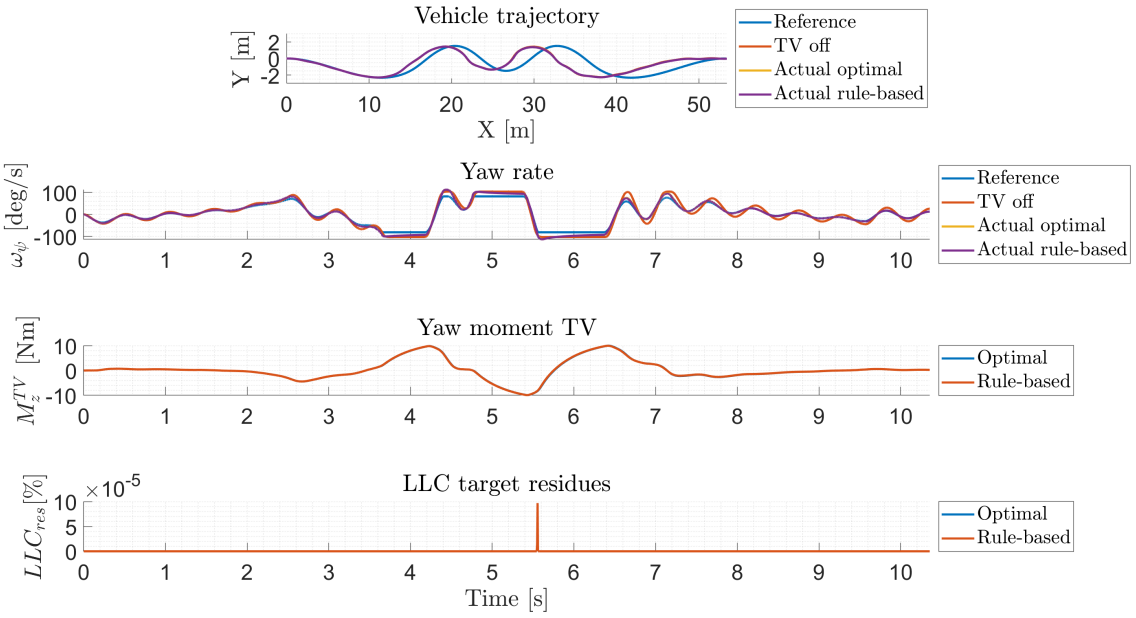

Figure 25: *Verification results.*

The trajectories that the vehicle undertakes, both with the TV on and off, are shifted with respect to the reference one and overlap. This shifted trend is due to the limited performance of the driver model.
The control system brings the yaw rate of the vehicle close to the reference as intended, even though this example is not meant to demonstrate the performance of the system yet. Indeed, the vehicle with the TV off shows behavior similar to that of the vehicle with the TV on, considering the small influence that the TV has at this low speed.

The LLC correctly deploys the requested yaw moment.
the LLC target residues are practically negligible, meaning that both the LLC logics satisfy the set requirements.
It is evident that the results of optimal control and rule-based control practically overlap. This behavior is common in a wide range of scenarios. For this reason, from now on, the adopted LLC logic will be rule-based.

8.5 Calibration

Since the proportional term of the PID controller for the ULC has proven to be the most influential factor in the yaw error correction, it is the only one that will be implemented.
Therefore, the parameter to be calibrated is the proportional gain (P_{ULC}). The sliding mode gain (Ksm) is not tunable through simulation, as it addresses the external disturbances affecting the vehicle that are not modeled in this case. Therefore, its calibration must be undertaken on track.
To undertake a proper calibration, the minimization function `fmincon` from `Matlab` is exploited.
The parameter to be minimized is the rms error of the trajectory defined as:

$$rms(e_t) = rms(e_h) + rms(e_y) \tag{64}$$

where e_h and e_y have been defined in Section 8.2.
The result of the calibration process is:

$$P_{ULC} = 80;$$

8.6 Validation

During the validation phase, all the tests introduced in Section 8.1 are undertaken. For each test, the trend of the states associated with the KPIs (Section 8.2) is shown, and the KPI values are collected in a table.

The first state to be tracked is the lateral acceleration:

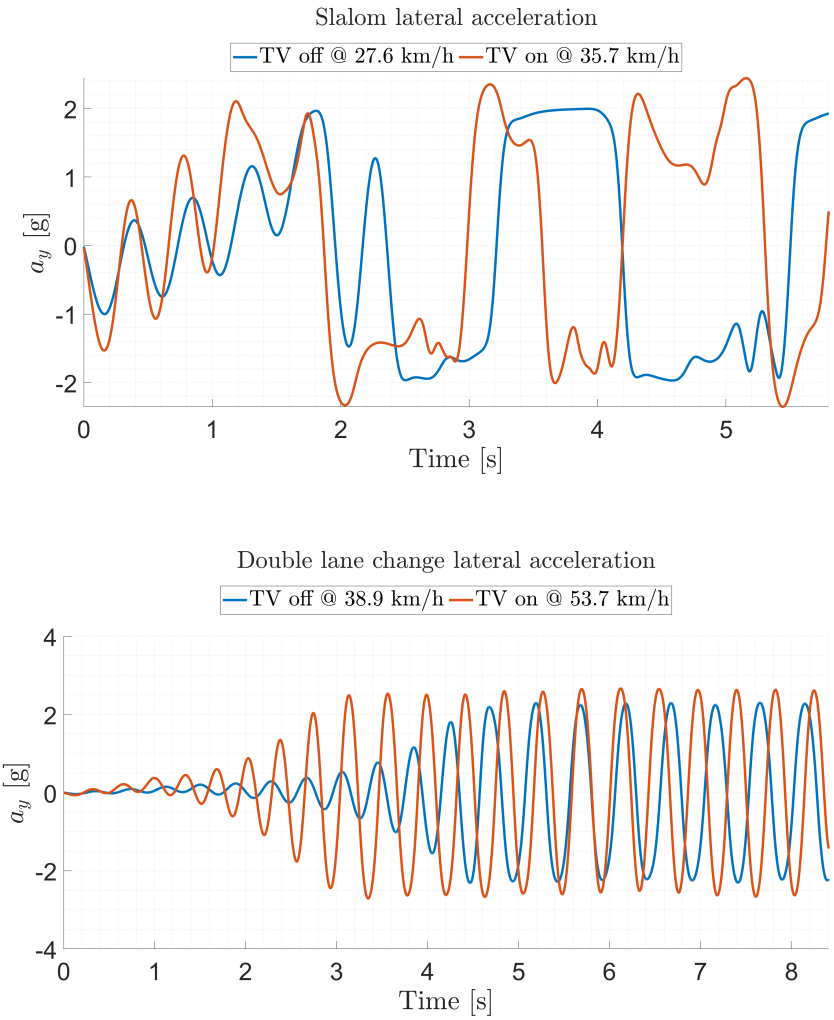

Figure 26: *Lateral acceleration trend along the maneuvers.*

To prove the performance enhancement associated with the activation of the Control System, different simulations have been carried out. The goal is to understand for which value of longitudinal speed the vehicle completely misses the reference trajectory. To perform this task, the trajectory error (e_t) is tracked.
From simulations, it has been observed that the vehicle completely misses the reference trajectory for the following values of e_t:

- slalom: $e_t = 4$;
- double lane change: $e_t = 0.36$;

These values differ from one another due to the different dynamics involved in the maneuvers.
The results of the longitudinal speed limits from simulations are specified in Figure 26 for each combination of maneuver and TV state.

The lateral acceleration signal presents significant oscillations during the double lane change maneuver. This behavior is due to the lack of stability performance from the vehicle controller, which attempts to keep the vehicle on its trajectory. Therefore, the maximum lateral acceleration value is computed as a mean over the transient time to filter out the effects of undesired oscillations. The same observations regarding the double lane change hold for the following two KPIs.
To summarize the outcome from this first KPI, the TV visibly enhances the lateral performance of the vehicle in both scenarios.

Moving on, the next KPI is the average yaw index. The trend of the associated state is presented here:

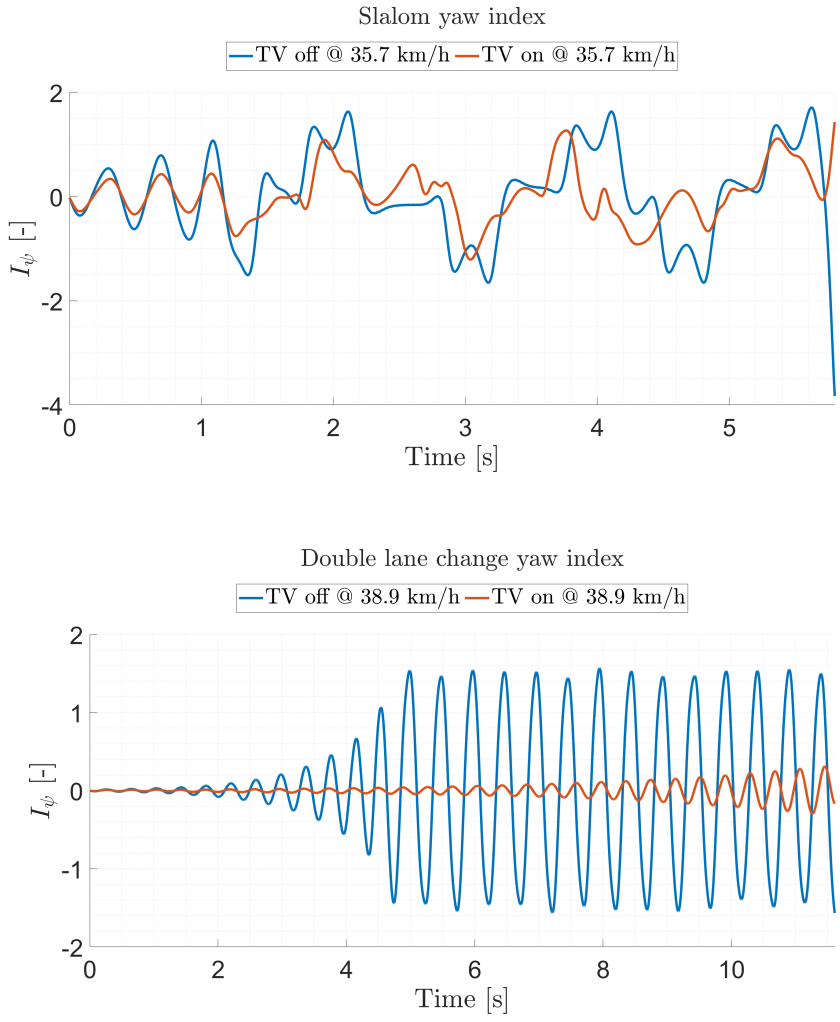

Figure 27: *Yaw index trend along the maneuvers.*

Unlike lateral acceleration, the trends for each maneuver are shown at the same vehicle speed. This choice is intended to demonstrate that the control system improves handling under the same driving conditions. Indeed, when the TV is activated, the

state trend is strongly dampened, meaning that the vehicle tends to be closer to the neutral steering condition, which is optimal for handling performance.
The last state under focus is the trajectory error at a certain speed:

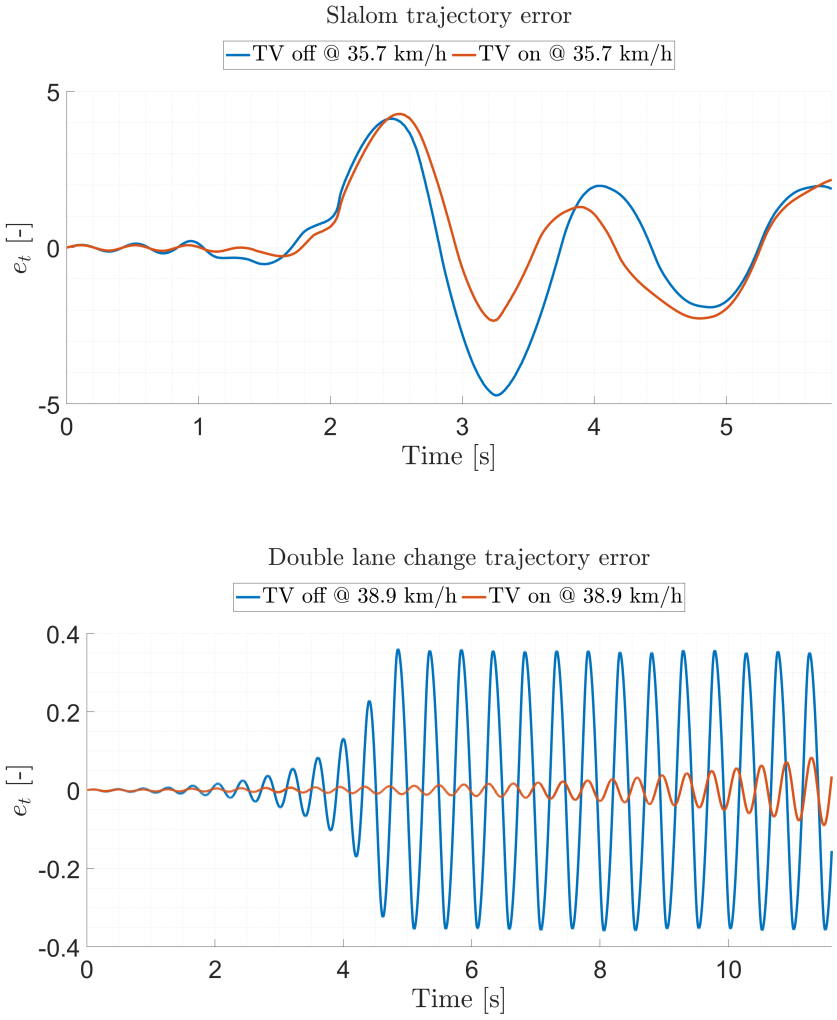

Figure 28: *Yaw index trend along the maneuvers.*

When the Control System is turned on, the trajectory error is significantly lower, meaning that the vehicle better maintains its reference trajectory. This outcome is important not only for performance's sake but also for safety purposes: the vehicle is more stable under tricky driving scenarios. This observation is strengthened by the previous results on the yaw index, which demonstrate the achievement of a more neutral steering behavior.

The KPIs associated with the just presented states trend are collected in the following table:

Table 2: *TV validation results.*

Maneuver	**TV state**	a_y^{MAX}	I_ψ^{RMS}	e_t^{MAX}
Slalom	OFF	2.0 g, @27.6 km/h	0.9, @35.7 km/h	4.7, @35.7 km/h
	ON	2.4 g, @35.7 km/h	0.5, @35.7 km/h	4.3, @35.7 km/h
Double lane change	OFF	1.4 g, @ 38.9 km/h	0.9, @ 38.9 km/h	0.4, @ 38.9 km/h
	ON	1.6 g, @ 53.7 km/h	0.1, @ 38.9 km/h	0.1, @ 38.9 km/h

To quantify and highlight the enhancement achieved by the implementation of the TV Control System, these results are shown as relative improvement with respect to the passive vehicle:

Table 3: *TV validation relative results.*

Maneuver	a_y^{MAX}	I_ψ^{RMS}	e_t^{MAX}
Slalom	$\uparrow$ 20%	$\downarrow$ 44%	$\downarrow$ 9%
Double lane change	$\uparrow$ 12%	$\downarrow$ 89%	$\downarrow$ 75%

Table 4: *TV validation relative results.*

Maneuver	a_y^{MAX}	I_ψ^{RMS}	e_t^{MAX}
Slalom	$\uparrow$ 20%	$\downarrow$ 44%	$\downarrow$ 9%

The last test undertaken is the step steer maneuver. It allows for the characterization of the yaw damping performance of the Control.
The results from this maneuver are shown in the following figure:

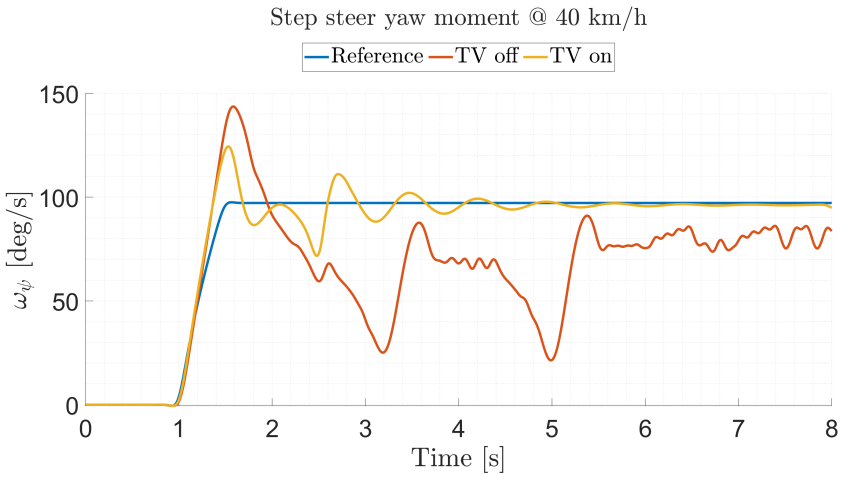

Figure 29: *Step steer yaw moment.*

Three different KPI values summarize the vehicle's response to this maneuver:

Table 5: *Yaw damping characterization.*

TV state	Rise time	Overshoot	Steady-state error
OFF	1.03s	80%	18%
ON	1.08s	29%	1%

The rise time indicates how quickly the vehicle's response is to the driver command input (steering wheel). The overshoot, instead, provides an indication of how stable the vehicle is during the maneuver. Finally, the steady-state error indicates the difference between the vehicle current rotation rate and its reference.
The outcome of this analysis is that the Control System is able to better stabilize the vehicle during a transient maneuver, leading it to a more optimal handling state, despite a slightly slower response at the inception of the maneuver itself.

To conclude, a track testing session has been undertaken; however, the time available has been a limiting factor when it comes to carrying out the planned tests. Therefore, only data from a slalom maneuver, with the Control System turned on, are analyzed:

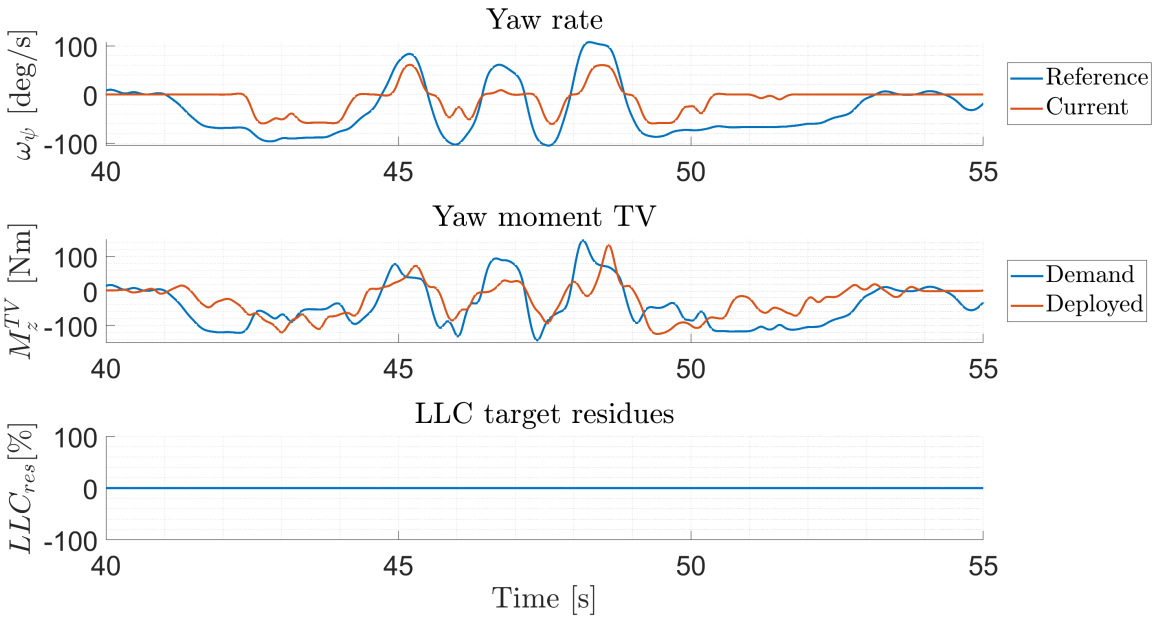

Figure 30: *Track test results for a slalom maneuver, where the current state signal refers to the measured one and the reference is the signal generated by the Control System.*

It is evident how the Control System correctly tries to follow the reference yaw rate, accordingly deploying a yaw moment. At the same time, the residues of the LLC target are practically null, meaning the LLC logic is functioning correctly.
The difference between the actual yaw rate and its reference is not necessarily caused by a lack of performance of the Torque Vectoring; rather, it can be related to other modules within the torque path, which might operate incorrectly with the TV, compromising its accuracy.

9 Vehicle speed measurement

The last topic addressed in this project is the implementation of a vehicle speed sensor. Despite the sensor not being utilized by this design version of the TV, its implementation will be crucial in a future logic yet to be developed.
Its application is not only limited to the enforcement of TV operations, as anticipated in Section 5.2, but it also represents a key feature for the development of:

- a high performance Traction Control System; the vehicle speed value is the basis for the computation of the wheel longitudinal slip;
- an accurate process for vehicle localization in driverless operations.

The team owns an optical speed sensor, the Kistler Correvit S-CE. Nevertheless, due to the aging of this sensor (production year 2001), it was difficult to determine whether its measurements were reliable. Thanks to the support received from the German company Sensoric Solutions, it has been possible to compare the Correvit with their brand-new product, OMS Race. This latter optical speed sensor has been tested on a wide range of series production vehicles, and it has also been internally calibrated at the end of the production phase. Therefore, the OMS has been considered a reference for measured vehicle speed data.
Both sensors have been mounted on the rear of the car. This solution is optimal for the current layout of the vehicle. The Correvit needed an external PCB to generate a positive DC voltage to allow the reading of lateral speed data in both positive and negative directions.

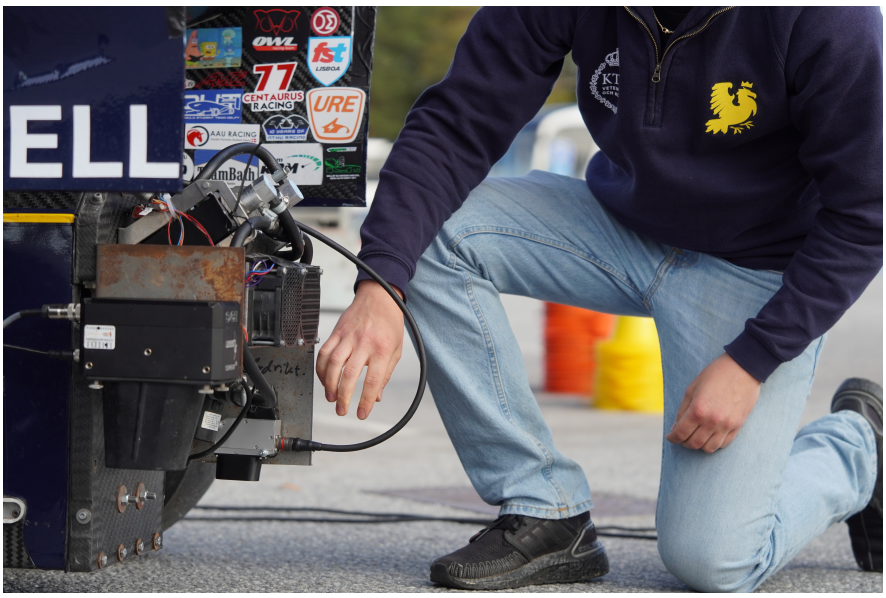

Figure 31: *Optical speed sensors mounting.*

Different maneuvers have been undertaken during the testing session, including slalom, double lane change and normal driving. The collected speed data follow:

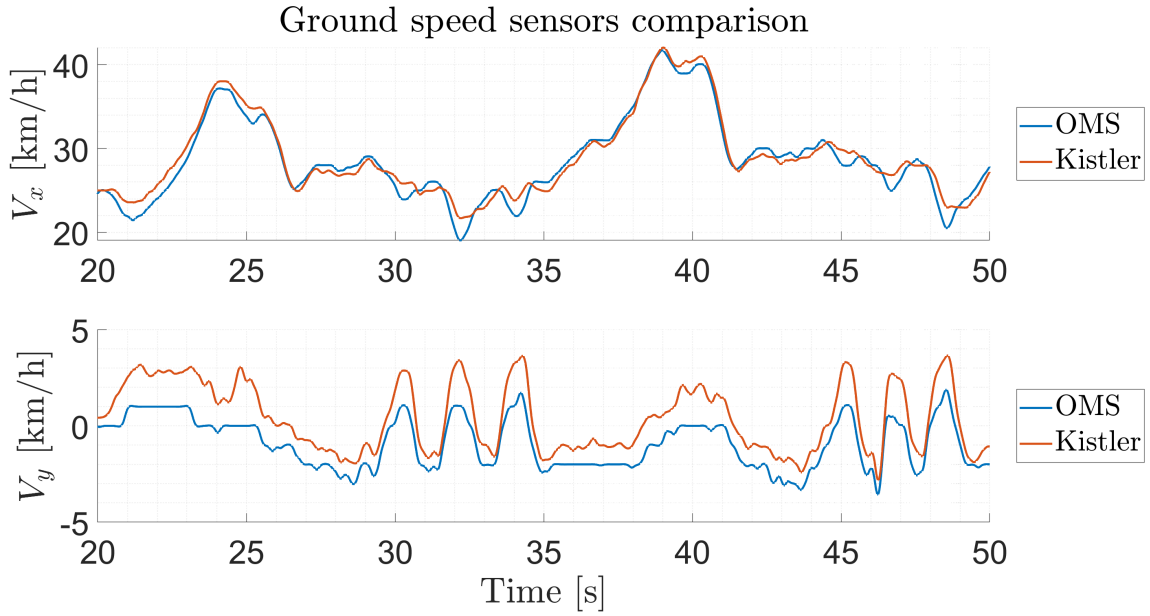

Figure 32: *Ground speed sensors comparison.*

In a post-processing phase, some noise present in the signals has been cleaned out for better observability.
It is evident that the longitudinal speed signals measured by the two sensors are very close, with the OMS being more accurate in capturing the variation in speed.
Instead, the lateral speed measured by the Correvit appears to have an offset with respect to the speed measured by the OMS. This difference might be related to the Correvit still needing improvement in the calibration of the integrated DC voltage.

To conclude, with some further work to be done, the Correvit appears to be a promising tool to implement in the vehicle to enhance its performance.

10 Conclusions

The development of the Torque Vectoring control system involved different engineering areas, including vehicle dynamics for the definition of the control system logic itself, control system theory for the implementation of a robust and high-performing actuation architecture, and mathematics and linear algebra for the implementation of complex mathematical models used to set up the optimization problem.
With respect to the two logics presented for the ULC, only one has been consistently carried on: the direct yaw control. To this logic, a simple proportional gain has been associated with the controller; however, a more advanced control technique, the sliding mode control, has been developed. Nevertheless, the validation of this last technique is not addressed in this project.
Regarding the two logics of the LLC, which are designed with the same target, despite being very different in their structure, they have proven to lead to the same results with satisfactory performance.
The Control System has been tested under different dynamic scenarios within a simulation environment. Eventually, it proved to lead to a considerable enhancement in the lateral dynamics performance of the vehicle, thereby improving safety as a consequence.
Finally, a track testing session proved the effective operation of the Torque Vectoring system according to its intended functions.

11 Future work

Regardless of the evidence of improvement in handling provided by this version of the Torque Vectoring system, different enhancements can still be achieved.
A list of the different points to be covered in future work is presented:

- as mentioned in Section 1.5, an accurate measurement of the vehicle lateral speed was not present. Therefore, considering a method to measure this quantity to be present in the future, an implementation of the vehicle side-slip angle in the control logic must be investigated;
- the driver and vehicle model must be improved to obtain more accurate results before the track testing sessions. The driver model should be able to control not only the lateral dynamic of the vehicle (e.g., steering wheel) but also the longitudinal dynamic of the vehicle (e.g., throttle and brake);
- the calibration and validation of the sliding mode controller have not been addressed, considering the lack of external disturbances in the simulation model. Thus, further investigations regarding the effect of this feature must be carried out;
- a complete track testing session, with all the maneuvers correctly undertaken, must be carried out for a complete correlation of real data with the simulation results;
- a different logic for the ULC can be studied, focusing more on the under-steering control of the vehicle, for instance, possibly exploiting the yaw index.

References

[1] E. Saykol, "An economic anlysis of software development process based on cost models," *International Conference on Eurasian Economies - At: Almaty*, Oct. 2012.

[2] M. Vignati, E. Sabbioni, and D. Tarsitano, "Torque vectoring control for iwm vehicles," 2016.

[3] S. Sakai, H. Sado, and Y. Hori, "Y. motion control in an electric vehicle with four independently driven in-wheel motors," Apr. 1999.

[4] L. D. Novellis, A. Sorniotti, P. Gruber, and A. Pennycott, "Comparison of feedback control techniques for torque-vectoring control of fully electric vehicles," Oct. 2014.

[5] P. Sun, A. S. Trigell, L. Drugge, and J. Jerrelind, "Comparison of feedback control techniques for torque-vectoring control of fully electric vehicles," Oct. 2014.

[6] T. Goggia, A. Sorniotti, L. D. Novellis, and A. Ferrara, "Torque-vectoring control in fully electric vehicles via integral sliding modes," Jun. 2014.

[7] M. Vignati, E. Sabbioni, and F. Cheli, "A torque vectoring control for enhancing vehicle performance in drifting," 2018.

[8] M. Asperti, M. Vignati, and E. Sabbioni, "On torque vectoring control: Review and comparison of state-of-the-art approaches," Feb. 2024.

[9] A. Ferrara, *Sliding Mode Control Handout*.

[10] MATHWORKS. (2025) What is quadratic programming? [Online]. Available: https://it.mathworks.com/discovery/quadratic-programming.html

[11] D. Arnström, A. Bemporad, and D. Axehill, "A dual active-set solver for embedded quadratic programming using recursive LDL^T updates," *IEEE Transactions on Automatic Control*, vol. 67, no. 8, pp. 4362–4369, 2022.

A Rule-based control algorithm

```
%% Preliminary distribution of the forces for each lateral side
   (left and right), starting from the torque limits
FxMaxSide = Tmax * 2 / taoGB / Rl; % [N]
FxMinSide = Tmin * 2 / taoGB / Rl; % [N]
FxMidSide = (FxMinSide+FxMaxSide)/2; % [N]
FxMax = Tmax/Rl/taoGB./[1/cos(SteeringAngleL);
   1/cos(SteeringAngleR); 1; 1];
FxMin = Tmin/Rl/taoGB./[1/cos(SteeringAngleL);
   1/cos(SteeringAngleR); 1; 1];

trqDemand = Tmax * 4 * Throttle; % [N*m] (total torque demanded
   by the driver)
trqWheels = trqDemand / taoGB;
Fx0 = trqWheels/ Rl; % [N] (total force demanded by the driver)
FxSide0 = [Fx0/2, Fx0/2]; % [L R] (total force demanded per
   side)

% Computation of the force to be be added/subtracted for each
   side:
dFx = Mz/t; % [N]
dFxR = dFx;
dFxL = dFx;

% Preliminary yaw moment distribution:
FxSideProv = [FxSide0(1)-dFxL, FxSide0(2)+dFxR]; % [L R]
Fprov = [FxSideProv(1)/2;FxSideProv(2)/2; ...
FxSideProv(1)/2;FxSideProv(2)/2] ...
.*[1/cos(SteeringAngleL); 1/cos(SteeringAngleR); 1; 1];
MzProv = [(-t/2*cos(SteeringAngleL)+lf*sin(SteeringAngleL)), ...
t/2*cos(SteeringAngleR)+lf*sin(SteeringAngleR)),-t/2,t/2]*Fprov;

% Check on the residual yaw moment:
deltaMz = Mz-MzProv;
dFxRecovery = deltaMz/t; % [N]
dFxR = dFxRecovery;
dFxL = dFxRecovery;
% Recovery of the residual yaw moment:
FxSideProv = [FxSideProv(1)-dFxL, FxSideProv(2)+dFxR]; % [L R]
```

```
33
34 %% Check of the preliminary set forces for each lateral side to
       verify if they respect the force bounds:
35 FxSide = FxSideProv;
36 side = [1, 2]; % [L, R]
37 % The TV operates mirrored for yaw moment values of opposite
       sign:
38 if Mz < 0
39     side = fliplr(side); % [L, R]
40 end
41
42 % The relative distance of the force demand from the mid point
       of the
43 % operational range allows to preview which saturation is
       reached before (upper or lower):
44 if Fx0/2 >= FxMidSide & FxSideProv(side(2)) >= FxMaxSide
45     % Upper saturation reached
46     FxSide(side(1)) = max(FxMinSide, FxSideProv(side(1)) -
           (FxSideProv(side(2))-FxMaxSide)); % Left side (for Mz>0)
47     FxSide(side(2)) = FxMaxSide; % Right side (for Mz>0)
48 elseif Fx0/2 < FxMidSide & FxSideProv(side(1)) < FxMinSide
49     % Lower saturation reached
50     FxSide(side(1)) = FxMinSide; % Left side (for Mz>0)
51     % When lower saturation is reached, the other side recovers
           the
52     % deficit until a threshold, to not overcome the driver
           demand:
53     FxSide(side(2)) = min(FxMaxSide, FxSide0(side(2)) +
           (FxSide0(side(1))-FxMinSide)); % Right side (for Mz>0)
54 end
55
56 %% Longitudinal distribution of the forces (front to rear):
57 Fx = [FxSide(1)*FzRatioL/(1+FzRatioL);
       FxSide(2)*FzRatioR/(1+FzRatioR); FxSide(1)/(1+FzRatioL);
       FxSide(2)/(1+FzRatioR)]; % [N] [FL, FR, RL, RR]
58
59 % Check on the boundaries to compensate saturation:
60 if Fx(1)>FxMax(1)
61     Fx(3) = max(FxMin(3), Fx(3)+(Fx(1)-FxMax(1)) );
62     Fx(1) = FxMax(1);
```

```
63  end
64  if Fx(3)>FxMax(3)
65      Fx(1) = max(FxMin(1), Fx(1)+(Fx(3)-FxMax(3)) );
66      Fx(3) = FxMax(3);
67  end
68  if Fx(2)>FxMax(2)
69      Fx(4) = max(FxMin(4), Fx(4)+(Fx(2)-FxMax(2)) );
70      Fx(2) = FxMax(2);
71  end
72  if Fx(4)>FxMax(4)
73      Fx(2) = max(FxMin(2), Fx(2)+(Fx(4)-FxMax(4)) );
74      Fx(4) = FxMax(4);
75  end
76
77  % Check on the residual yaw moment:
78  Fprov = Fx.*[1/cos(SteeringAngleL); 1/cos(SteeringAngleR); 1;
        1];
79  MzProv = [(-t/2*cos(SteeringAngleL)+lf*sin(SteeringAngleL)), ...
80  (t/2*cos(SteeringAngleR)+lf*sin(SteeringAngleR)), ...
81  -t/2,t/2]*Fprov;
82  deltaMz = Mz-MzProv;
83  dFxRecovery = deltaMz/t; % [N]
84  dFxR = dFxRecovery;
85  dFxL = dFxRecovery;
86  % Recovery of the residual yaw moment by the rear axle:
87  Fx(3) = Fx(3)-dFxL;
88  Fx(4) = Fx(4)+dFxR; % [L R]
89  % Check on the boundaries to compensate saturation:
90  if Fx(3)>FxMax(3)
91      Fx(1) = max(FxMin(1), Fx(1)+(Fx(3)-FxMax(3)) );
92      Fx(3) = FxMax(3);
93  end
94  if Fx(4)>FxMax(4)
95      Fx(2) = max(FxMin(2), Fx(2)+(Fx(4)-FxMax(4)) );
96      Fx(4) = FxMax(4);
97  end
98
99  %% Final torque values determination:
100 T = Fx*Rl*taoGB.*[1/cos(SteeringAngleL); 1/cos(SteeringAngleR);
        1; 1];
```

```
101 T = min(T,Tmax);
102 T = max(T,Tmin);
```

B Algebraic approach for the QP terms

A quadratic cost function can be formulated analytically in the following way:

$$J(x) = \tfrac{1}{2}\, x^\top \cdot H \cdot x + f^\top \cdot x$$

where H is the Hessian matrix, f is the gradient vector, and x is the state vector. The first step of this formulation is the definition of the vectors making up the Hessian matrix:

$$Q_1 = \begin{bmatrix} F_z^{RL} & 0 & -F_z^{FL} & 0 \end{bmatrix}$$
$$Q_2 = \begin{bmatrix} 0 & F_z^{RR} & 0 & -F_z^{FR} \end{bmatrix}$$
$$Q_3 = \sqrt{\gamma} \cdot \begin{bmatrix} 1 & 1 & 1 & 1 \end{bmatrix}$$

The Hessian matrix is then defined as:

$$H = Q_1^\top \cdot Q_1 + Q_2^\top \cdot Q_2 + Q_3^\top \cdot Q_3.$$

Expanding each term of H:

$$Q_1^\top \cdot Q_1 = \begin{bmatrix} (F_z^{RL})^2 & 0 & -F_z^{RL}F_z^{FL} & 0 \\ 0 & 0 & 0 & 0 \\ -F_z^{RL}F_z^{FL} & 0 & (F_z^{FL})^2 & 0 \\ 0 & 0 & 0 & 0 \end{bmatrix},$$

$$Q_2^\top \cdot Q_2 = \begin{bmatrix} 0 & 0 & 0 & 0 \\ 0 & (F_z^{RR})^2 & 0 & -F_z^{RR}F_z^{FR} \\ 0 & 0 & 0 & 0 \\ 0 & -F_z^{RR}F_z^{FR} & 0 & (F_z^{FR})^2 \end{bmatrix},$$

$$Q_3^\top \cdot Q_3 = \gamma \cdot \begin{bmatrix} 1 & 1 & 1 & 1 \\ 1 & 1 & 1 & 1 \\ 1 & 1 & 1 & 1 \\ 1 & 1 & 1 & 1 \end{bmatrix}.$$

Combining all the terms, the final expression of the Hessian matrix is:

$$H = \begin{bmatrix} (F_z^{RL})^2 + \gamma & \gamma & -F_z^{RL} \cdot F_z^{FL} + \gamma & \gamma \\ \gamma & (F_z^{RR})^2 + \gamma & \gamma & -F_z^{RR} \cdot F_z^{FR} + \gamma \\ -F_z^{RL} \cdot F_z^{FL} + \gamma & \gamma & (F_z^{FL})^2 + \gamma & \gamma \\ \gamma & -F_z^{RR} \cdot F_z^{FR} + \gamma & \gamma & (F_z^{FR})^2 + \gamma \end{bmatrix}.$$

The gradient vector formulation follows:

$$f = -T_{DMD} \cdot \gamma \cdot \begin{bmatrix} 1 & 1 & 1 & 1 \end{bmatrix}^\top$$

Expanding $J(x)$ explicitly:

$$J(x) = \frac{1}{2}\begin{bmatrix} T_{FL} & T_{FR} & T_{RL} & T_{RR} \end{bmatrix} \cdot H \cdot \begin{bmatrix} T_{FL} \\ T_{FR} \\ T_{RL} \\ T_{RR} \end{bmatrix} + f^{\top} \cdot x.$$

After developing the expression and undertaking all possible algebraic simplifications, the final cost function expression is reached:

$$J(x) = \frac{1}{2}\Big[(T_{FL}\cdot F_z^{RL} - T_{RL}\cdot F_z^{FL})^2 + (T_{FR}\cdot F_z^{RR} - T_{RR}\cdot F_z^{FR})^2 + \gamma\cdot\Big(\sum_i T_i\Big)^2 - 2\cdot\gamma\cdot T_{DMD}\cdot\sum_i T_i\Big].$$